Synthesis and Characterization of the Iron, Yttrium and Chromium Oxides Thin Films Using AACVD for their PEC Applications.

by

Rafia bintay Yousaf

Reg. # 00000172942

A thesis submitted in partial fulfillment of the requirements

for the degree of **Master of Science** in

Chemistry

Supervised by: Dr. Mudassir Iqbal

Department of Chemistry

School of Natural Sciences

National University of Sciences and Technology

H-12, Islamabad, Pakistan

2019

FORM TH-4

National University of Sciences & Technology

MS THESIS WORK

We hereby recommend that the dissertation prepared under our supervision by: Rafia Bintay Yousaf, Regn No. 00000172942 Titled: Synthesis and Characterization of Iron, Yttrium and Chromium Oxide Thin Films Using AACVD for Their PEC Applications Be Accepted in partial fulfillment of the requirements for the award of **MS** degree.

Examination Committee Members

1. Name: DR. AZHAR MAHMOOD Signature: _____

2. Name: DR. MUHAMMAD ADIL MANSOOR Signature: _____

External Examiner: DR. SHAHID ALI KAHAN Signature: _____

Supervisor's Name: DR. MUDASSIR IQBAL Signature: _____

Co-Supervisor's Name: PROF. M. MAZHAR Signature: _____

_____ 31/12/2019

Head of Department Date

COUNTERSINGED

Date: 31/12/2019

Dean/Principal

THESIS ACCEPTANCE CERTIFICATE

Certified that final copy of MS thesis written by **Ms. Rafia Bintay Yousaf** (Registration No. **00000172942**), of **School of Natural Sciences** has been vetted by undersigned, found complete in all respects as per NUST statutes/regulations, is free of plagiarism, errors, and mistakes and is accepted as partial fulfillment for award of MS/M.Phil degree. It is further certified that necessary amendments as pointed out by GEC members and external examiner of the scholar have also been incorporated in the said thesis.

Signature: _____

Name of Supervisor: Dr. Mudassir Iqbal

Date: 31-12-2019

Signature (HoD): _____

Date: 31/12/2019

Signature (Dean/Principal): _____

Date: 31/12/2019

Dedication

Dedicated to my beloved Grand Father Jamal Din (Late) and my loving Parents Mr. and Mrs. Muhammad Yousaf Naz

Acknowledgements

*I am indebted to the **Allah Almighty** the supreme power for blessing me with the ability, determination and potential to complete my thesis work. I pay my sincere and humblest thanks to the Rahmatul lil-'Aalameen **Hazrat Muhammad (Peace be upon him**)who urges his believers to seek out knowledge.*

*I am profoundly grateful to my research supervisor **Dr. Mudassir Iqbal** for all his, motivation, and guidance during my research work. His invaluable knowledge has always motivated me.*

*I am very thankful to my Co Supervisor **Prof. Muhammad Mazhar** for his supervision, inspiration and timely response to the problems which I encountered during my research period.*

*I am also obliged to my GEC members **Dr Adil Mansoor** and **Dr. Azhar Mehmood** for their instructions and constructive criticism for improvement. My genuine thanks go to the Head of Chemistry department, **Dr. Muhammad Arfan** for supporting me morally. I am thankful to Principal SNS **Dr Rashid Farooq** for listening to our research related problems and accommodating us with the best possible solutions. I also acknowledge **NUST (National University of Science and Technology),** all its departments **(SCME, SNS and CASEN), National Center for Physics and NINVAST** for the facilities and technical support.*

*I would like to thank to **Dr.Shahzad Abubakar** from **NCP** for helping me out and guiding me with my lab work and thesis writing.*

*I want to extend my heartful gratitude to my family namely my parents (Mr. and Mrs. **Muhammad Yousaf Naz**) and my brothers (**Muhammad Umer bin Yousaf** and **Muhammad Talha bin Yousaf**) for their protection, care, love, financial and moral support and for always believing in me regardless of what happen and providing me with valuable advice throughout my research work .I might not be able to carry out this work without their encouragement.*

*A special thanks to my best friend **Sara Ali** and my colleagues and friends **Sadaf Pervaiz**, **Anam**, **Farah shabbir**, **Wajiah** and **Huma** for their courage, help and motivation during my study.*

Lastly, I want to thank my aunts, uncles and cousins for their concern and prayers.

Abstract

It is a dire need for the development of materials that can generate energy from renewable resources, which are helpful to meet the future energy challenges as well as to address global warming. In the present research project, we have studied an efficient method for hydrogen production through water splitting using solar irradiation. We have developed the nanostructured transition metal oxides thin films of yttrium (Y), chromium (Cr) and iron (Fe) from their single source precursors using in-house build aero-sol assisted chemical vapor deposition technique. The as-fabricated thin films were characterized for their structural, optical, morphological, and electrochemical properties using XRD, FESEM, EDS, FTIR, UV and LV measurements. Furthermore, the as-fabricated thin films were applied as working electrode to test their photoelectrochemical water splitting response under xenon lamp irradiation using linear voltammetry. The thin films showed prominence response for PEC applications. Apart from this, it is interesting to mention that we have tried to develop the single source precursor of transition metals i.e. gadolinium, europium, gallium, yttrium and chromium, corresponding to the development of their respective metal sulfide electrodes for PEC study. Unfortunately, we could not be successful in the synthesis of these precursors for metal sulfide thin films fabrication. The detail of the unsuccessful reactions and possible reasons have been discussed in the experimental section of the thesis.

Table of Contents

List of Figures

List of Tables

List of abbreviations

^{o}C	Degree Centigrade
EDS	Energy Dispersive X-ray Spectroscopy
Eg	Energy Band Gap
e^{-}	Electron
e.g.	Example gratia (For example)
eV	Electron Volts
FTIR	Fourier Transform Infrared Spectroscopy
FTO	Fluorinated Tin Oxide
g	Gram
g/mol	Gram per Mole
i.e.	Id est (That is)
kJ/g	Kilo joule per gram
mA/cm^2	milli ampere per centimeter square
mg	Milligram
mL	Milliliter
mmol	Millimol
mV	Millivolt
Na (dtc)	Sodium diethyldithiocarbamate
nm	Nano-meters
Ppts	Precipitate
FESEM	Field Emission Scanning Electron Microscopy
UV-VIS Spectroscopy	Ultra Violet-Visible Spectroscopy

XRD	X-ray Diffraction

Chapter No. 1

Introduction

1.1Energy Crisis

Energy is inimitable need of life. Incessant energy supply is required for survival of living organism in the universe[1]. It is essential for social and economic escalation of any nation. With the passage of time; as human society has revolutionized; energy utilization has also increased. Energy is needed for the smooth running of industries, domestic and agricultural and transportation activities[2]. It power computers, medical equipment, electronics, communications, heating and cooling appliances etc.[3]. This world would be a freezing and dark without energy. Energy is utilized to perform the daily life human activities for example: preparing food, warming homes, running vehicles and producing merchandises[4]. Human of present century are facing energy crisis Energy crisis is economic problem due to the narrowed stock of energy resources and continuous usage, which causes depletion of these shrinking fossil fuels[5]. Shortage of energy resources results in the rise of fuel prices. This largely effect the growth of the nation. At present, major portion of energy is obtained by using fossil fuels[6]. Fossil fuels are non-renewable resources and thousands of centuries are needed for their development. Subsequently, their reserves are dwindling at higher rate as compared to the rate of formation of new ones. These resources are used to endure the energy demands worldwide[7]. Production, use and transmission of fossil fuel also causes the environmental degradation. Burning of this carbon-based fuel is responsible for production of air pollutants, such as, heavy metals and sulfur oxides, as well as for the emission of CO_2, the notorious greenhouse gas broadly considered as the culprit of worldwide climate change[8]. Global warming and environmental depletion are more alarming issues because of the continuous source of greenhouse gases into natural habitat and environment.

1.2 Possible Solution:

To meet with these challenges, development of environment friendly, proficient, sustainable and cost-effective energy sources is employed. Apart from these policies for conversion, storage and conservation of energy is pressing necessity[9]. For this purpose, solar cells, batteries, capacitors, super conducting magnets, thermostat, smart windows, photovoltaics cell, fuel cell, electrochemical energy storage, photoelectrochemical(PEC) energy conversion and various other devices are used[10][11][12]. One approach for the solution of energy crisis is, to increase the efficiency in utilization, transmission and production of the residual fossil fuels whereas reduce their harmful influences on the atmosphere. Secondly, technologies and set-ups must be improved or developed which are beneficial in the smooth progression towards the renewable and substituting energy sources i.e., , hydropower solar energy, nuclear power, wind power, geothermal energy, biofuels and biomass etc. [13].

1.3Photelectro Chemical Water Splitting for Hydrogen Production:

Hydrogen is expected to be utilize as the potential energy carrier and energy source for future energy requirement. It is the lightest element having the density equals to 0.0695 corresponding to the air and has physical characteristics of being a tasteless, odorless and colorless gas[5]. It is efficient fuel which is free of the hazardous gasses emission to the environment and can be used in fuel cells for the production of electricity. Greater conversion efficiencies may be accomplished by using hydrogen as a fuel either in fuel cell or combustion mode instead of fossil fuels-based combustion engine. Energy obtained from hydrogen i.e. about 122 kJ/g that is nearly 2.75 times higher than the energy produced from gasoline Vehicles, in which hydrogen fuel is used, have considerably reduced the need of fossil fuels and evidently lessen tailpipe emissions of harmful materials[14]. Hydrogen can be regarded as efficient, green and clean fuel only if it is generated by using renewable resource of energy. Scientists are trying to fabricate economical, effectual and sustainable techniques to produce hydrogen[4]. Sunlight is a valuable source of renewable energy that can provides relatively cheaper and cleaner energy for prolonged period of time[15]. Amount of solar energy provided by sun is equal to 3.8×10^{23} W. Which is much higher than the total amount of energy uses in the world[16]. Another notable source of renewable energy which is present in a large amount is water as it covers almost 70% of earth surface[17]. One of the clean, cheaper and ecologically friendly method for hydrogen

production is from water by using solar energy to split the water into its components i.e. hydrogen and oxygen. This technique of the development of hydrogen utilizing water and solar irradiation as primary source of energy through the splitting of water is known as photolysis. Remarkable work has been done in the field of photolysis after the first innovation of photoelectrochemical mechanism by Honda and Fujishima[18]. Their work was initially published in 1972. Photoelectrochemical water splitting is resemble in mechanism to photosynthesis occurs in plants during which CO_2 and water react in the presence of sunlight and as a result of redox reaction glucose and oxygen are produced. During the process of water splitting using PEC electricity generated by photovoltaic schemes is directly used to produce oxygen and hydrogen within one prototype device, the photoelectrochemical cell (PEC)[19]. Photoelectrochemical (PEC) system is basically an electrochemical system which is coupled with solar system, in which interactions between electrochemical reaction and optical photons take place[20].

Two-electrode system of PEC water splitting is shown in Figure 1 In this schematic illustration, photoelectrode of semiconductor material is dipped in an electrolyte solution which is light sensitive. This photoelectrode is connected to counter electrode which is metallic through electrical wiring. When this system is exposed to sunlight, electrons generated through photons are move towards conduction band from valance band. Thus, generation of electron and hole pair upon the surface of semiconductor is resulted which electrochemically interact with the ionic species present inside the liquid solution at the liquid/solid interfaces. Photoexcited holes and electrons at the surface of anode and cathode are used for oxidation and reduction reactions, respectively. In the photoanode system has shown where oxygen is evolved at the semiconductor surface and holes are inserted into the solution, while at the counter-electrode; hydrogen is evolved where photoexcited electrons are absorbed. Contrarily, in photocathode systems, at the surface of semiconductor H_2 evolved through reduction reactions where electrons are inserted into solution and oxygen is evolved due to oxidation reaction at the counter electrode. [21]. Transfer of holes/electrons among anode and cathode took place by using conductive pathway (e.g. wire), whereas H^+ ion moves toward cathode from anode by passing through the aqueous solution. The reaction rate for oxidation and reduction reactions

during PEC water splitting must be same otherwise imbalance in charges at the interface of electrodes will cause the reaction to slow down or even hinder the complete process[22].

1.4 Aerosol Assisted Chemical Vapor Deposition:

Chemical vapor deposition (CVD) is the technique which is employed for the development of thin film via the chemical interactions among constitute particles. These particles are in vapor forms which interact chemically and deposited in the form of solid films at or near the surface of supportive substrate. Using CVD, thin films of high purity, uniform composition and higher stability cab be synthesized which can be used in different types of materials which are critical to modern day technology. CVD is useful for the film fabrication of both complex and simple compounds generally at low temperature. Chemical composition and physical structure and can both be altered by switching either the conditions of deposition or chemistry of reaction[23]. Types of Chemical reactions occur during the process of CVD include: oxidation, reduction, thermal decomposition/ pyrolysis, carbide and nitride formation, hydrolysis, disproportionation, synthesis reactions, and chemical transport. In a complex reaction, to produce specific end products, more than one type of reactions is involved which proceed in a series of steps. CVD is used for the thin film fabrication of vast range of compounds and elements. Organic inorganic and organometallic reactants can be employed as preliminary materials. For CVD gases are the best choice as they can be promptly metered and distributed towards the reaction chamber. Reactants in liquid or solid forms must be converted into vapors at temperatures where decomposition can be prevented. After the formation, these vapors are shifted inside the reactor with the help of a carrier gas by passing across the heating pipes. Metal oxides thin films prepared by using CVD are corrosion resistant and is used in various application[24] [25].

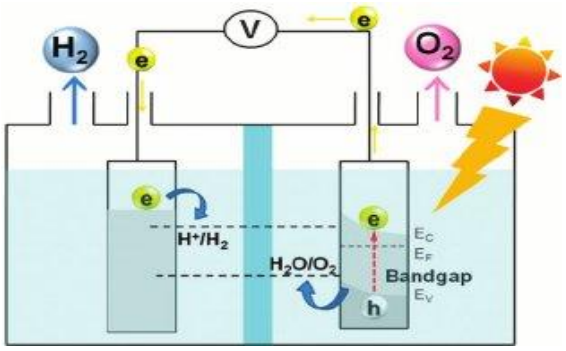

Figure 1 Basic principle of the photoelectrochemical water splitting and generation of hydrogen and oxygen on respective electrodes

[reproduced with permission from[26]].

In aerosol assisted chemical vapor deposition (AACVD) process precursor solution is converted to an aerosol haze, these vapors are then transferred to heating chamber through a carrier gas, where heated substrate are located and deposition take place. (Figure 2) As the aerosol reaches towards substrate chances of the occurrence of various prospects are present[27]. Most simple and efficient is when solvent evaporates totally from the droplet and molecules of precursor remained inside gas phase, which adsorbed upon the surface and results in the development of thin film over substrate. Second possibility which is rather complex is of partial evaporation due to which some amount of solvent stays upon the surface and results in direct contact with the surface. This phenomenon usually occurs in spray pyrolysis deposition method, in which droplets of aerosol are scattered directly upon the surface with higher speed then AACVD, due to which particle cannot gain enough time for complete evaporation[28].

In AACVD, solvent must be passed slowly around the warmed substrate so that it can be evaporated completely before moving towards the heated surface. Another possibility is of the homogenous reaction among the precursor either in solution-phase or gas phase before the heterogeneous deposition. Actually, it is probable statistically that all three of these phenomena are occurring in different combinations near the surface of the substrate[29].

1.4.1 Aerosol Generation:

Three methods are employed for the creation of aerosol, called as atomization or aerosolisation[30].

1.4.1.1Ultrasonic Aerosol Production:

It involves the generation of aerosol via ultrasonic vibrations. For this piezoelectric transducer is kept under the liquid. Then electric field of high frequency is provided to this transducer as a result ultrasonic vibration are produced. Ultrasonic waves are responsible for production of aerosol droplets when passed through the liquid. This technique is usually used in laboratories to produce aerosol for AACVD processes. This method is used for thin films deposition discussed in this work. (Figure 3)

1.4.1.2 Pneumatic Aerosol Jet:

In this process aerosol jet is produced by moving the liquid into a narrow space, where stream of condensed gas collides to it with high-velocity and results in the formation of mist of droplets. 1.4.1.3 Electrostatic atomization:

During this process electric current is applied near the spray nozzle. At the surface of the solution droplet of liquid is generated by its breakdown through the electrostatic charges.

1.4.2 Droplet Evaporation:

Concentration and size of the drops is inversely related to the time needed for saturation of gas. High concentration or large size droplets will cause the gas to saturate prior to the complete evaporation of droplets. That is why, thinner droplets are better choice. Evaporation of charged droplets is faster as compare to the uncharged droplets. Because of the repulsive forces among these droplets and charged surface. These repulsive forces take over the attractive surface tension[31].

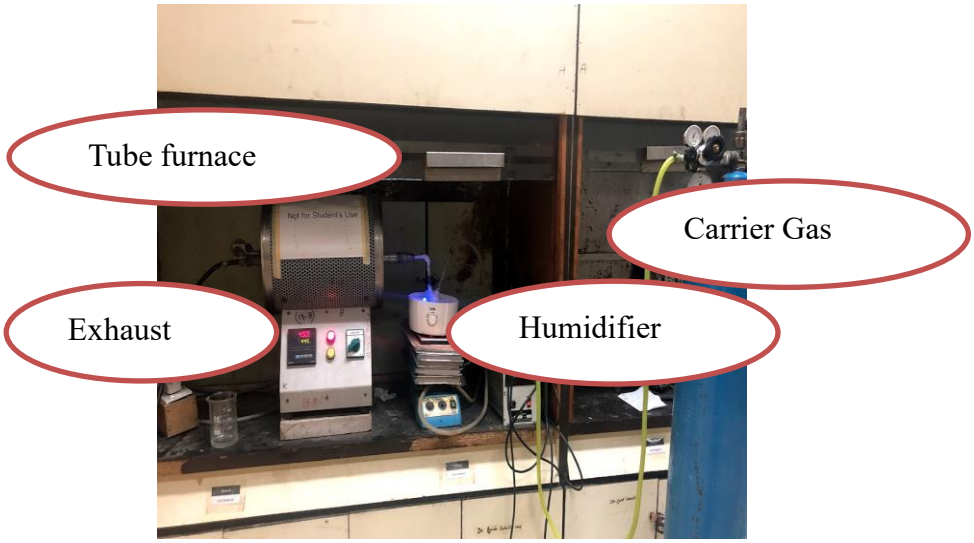

Figure 2 In-house designed Aerosol assisted chemical vapor deposition assembly used for the fabrication of transition metal oxide thin films on FTO substrate using single source precursor

Figure 3 Working condition of Ultrasonic Humidifier for the generation of aerosol during thin films fabrications.

Precursor requirement to be extremely volatile is eliminated in case of AACVD. This is due to the reason that precursors for AACVD just have the condition to be soluble in an appropriate solvent. This characteristic of AACVD made it enable to use for the deposition of large number of non-volatile precursors[32]. Secondly, reactor setup for the AACVD made of a simpler arrangement as compare to APCVD. The precursor solution is not heated before its

transformation inside the reactor instead it is nebulized. As well as pipes used for shifting of precursor also do not have to be heated to avoid condensation. Depositions may also be taken place in an open atmosphere. Due to all these properties this method of deposition is relatively cheaper. Another advantage it provides is the easy way to switch the surface morphology of the developed films. It can be done by altering the deposition parameters, for example, precursor, deposition temperature, substrate and solvent used to make solution of precursor. Due to which properties for example absorbance and conductivity which are linked with morphology can be tuned. Furthermore, AACVD is normally performed by using a single source, in which before the deposition the precursors molecules inside the solution undergo a considerable amount of mixing. This phenomenon provides an easy and better stoichiometry control when multi component materials are synthesized[33].

Chapter No. 2

Literature review

2.1 Methods for Production of Hydrogen:

Numerus technologies are reported to generate hydrogen from water which include electrolysis, radiolysis, photoelectrochemical(PEC), thermal and photobiological decomposition. Radiolysis is the method of hydrogen production through splitting of water by employing ionizing radiation. Numerous studies have been performed and published to analyze the efficiency for hydrogen generation through radiolysis of water[34][35]. For example, Frances et al had examined the effect of gamma radiations on water contained inside the zeolites. They performed their studies by varying the quantity of water inside zeolite. It was presented that the conversion efficiency of water to hydrogen was enhanced as compare to the bulk water radiolysis as a result of energy supplied by zeolites. It was depicted that high porosity in structure resulted in higher yield of hydrogen. In the given work the effect of gamma 137Cs irradiation upon zeolites 4A encompassing varying amounts of water was described. Impact of the ratio of water loading was focused. The improvement of hydrogen generation for diverse Zeolites 4A/ Water Systems (ZWS)in comparison to radiolysis of bulk water had been quantified and confirmed. The impact of the ratio of water loading by radiolysis upon the quantity of released hydrogen had been checked by employing two methods. A maximum yield of hydrogen through radiolysis was detected at a water loading ration of around 4 %. In this conformation, water was restrained inside the β cages and resulted in the sturdiest interaction with the zeolites which resulted in the enhanced radiolytic hydrogen generation through gamma irradiation[36]. Hydrogen production by thermal breakdown of water to is the method in which molecules of the water can be converted into hydrogen gas directly through thermal energy or via the help of other secondary transitional chemicals indirectly In theory, when water can directly split when provided the temperature above than 2000^{o}C, without the need of any other transitional chemicals[37]. For hydrogen production through thermal decomposition two-step cycles for water splitting are leading example which comprised of redox reactions of metals. These cycles typically comprise

of an endothermic reduction reaction for the production of oxygen and a hydrolysis reaction for production of hydrogen[38]. Kogan had described the procedure for H_2 production through water splitting using solar thermal energy as primary source. It presented an arduous technological task. However, when this process was syndicated with fuel cell technique greater efficiency for solar to hydrogen conversion was achieved. Water vapors were partly distanced into the solar reactor at very high temperatures reaches up to 2500 K. From the warmth mixture of the products yielded through the breakdown of H_2O, hydrogen was collected by utilizing gas diffusion across a permeable membrane[39]. Elif tezel et al. have generated hydrogen via the thermal decomposition of methane gas.in the presence of bimetallic Fe-Ni as catalyst. They used Al_2O_3 as secondary support. Thermal decomposition was done upon 700°Cat atmospheric pressure[40]. Biohydrogen or biological hydrogen is production of hydrogen through algae. Hydrogenase (H_2ase) is regarded as the key enzyme for hydrogen production of H_2 by using either photosynthetic green algae or some other progressive plants. This enzyme acts in anoxic condition, keeping in view this fact paramesh and colleagues had studied effect of tree oxygen removing species which was as sodium sulfite (Na_2SO_3), sodium metabisulfite ($Na_2S_2O_5$) and sodium dithionite ($Na_2S_2O_4$) independently combined with common tris-acetate-phosphate (TAP) medium for enhancement in yield of biohydrogen from Chlorococcum minutum a green alga. They attained the improvement in the production of biohydrogen for the first time via using sodium metabisulfite and sodium sulfite alongside algal cultures. Effectual enhancement in the overall production of H_2 via photobiological process was observed in C. minutum when above mentioned oxygen scavengers were added. On the other hand, efficiency of hydrogen production was low in the absence of these oxygen removing species. Among the studied three species, best results for hydrogen generation was showed in case of sodium sulphate, predominantly 0.8 mM $Na_2SO_3$was superlative .Possible reason for this might be because of greater oxidation state and comparatively larger electron negativity of Na_2SO_3[41].

The electrolytic splitting of H_2O for the concurrent synthesis of oxygen (O_2) and hydrogen (H_2) is basically an electrochemical procedure that utilizes electrical energy as the primary energy source for chemical reactions There are four types of methods given for electrolysis of water which are as (i) Alkaline water electrolysis (AWE) (ii) Microbial electrolysis cells (MEC) (iii)

Solid oxide electrolysis (SOE) (iv) Polymer electrolyte membrane (PEM) water electrolysis. Various types of electrodes and electrolytes are studied for water electrolysis[42]. Such as Hnát et al. had reported the fabrication and analysis of anion-exchange membrane (catalyst-coated and platinum-free) with a better functioning for electrolysis of alkaline water to attain hydrogen. For the deposition of electrodes hot plate spraying procedure was utilized and layer of thickness 35 or 120μm deposited upon an anion-selective polymeric surface of electrolyte membrane. These thicknesses were consequent to the load of catalyst equivalent to 2.5 and 10 mg cm^{-2} respectively. For electrolysis catalyst based on anode of $NiCo_2O_4$, cathode of $NiFe_2O_4$ along with anion selective binder of polymeric nature in the binder/ catalyst ratio equal to 1:9 were used. The response of the synthesized membrane-electrode design under alkaline water with the concentration varying from 1 to 15 wt% of potassium hydroxide KOH was calculated stability was verified by electrolysis test for 72-hours at current load equals to 0.25 Acm^{-2} of the synthesized assembly. The initial results for the electrolysis of the alkaline water cell showed both enhanced efficiency and stability of the developed assembly It was tested that no negative impact was shown on the electrolytic performance of alkaline water when the load of catalyst was reduced to 2.5 from 10 $mgcm^{-2}$. These results were compared to the activity of catalyst-coated conventional substrate[43].

Among these methods, PEC is an applicable and most suitable technique as it generates clean and cheap hydrogen and is consists of simple assembly. By product of radiolysis i.e. nuclear waste causes severe impacts on human health and environment. Photobiological water splitting pathway suffers from low production rates of hydrogen and due to the synthesis of oxygen during water splitting hydrogen generation reaction can be halted and is also dangerous when interact with hydrogen over a certain amount. The main limitations associated with thermal decomposition are the requirement of high temperature along with the less yield of hydrogen. The required temperature is very high to use for the commercial production of hydrogen. Furthermore, the product of thermolysis is the mixture of oxygen and hydrogen gas, that specifies a significant burst danger at such a preeminent temperature. The direct electrolysis of water is costly approach furthermore in this case maximum 60–66.5% efficiency is achieved and 33.5–40% electrical energy loss is occurred. The PEC water splitting approach, on one

hand eradicates the need of costly electrolyser and on the other hand enhances the conversion efficiency through the utilization of photon energy which further reduces the cost[44][45].

2.2 Devices Studied for PEC Water Splitting:

In recent times, semiconductor devices in various form, such as , powders, colloids and thin films, have been studied extensively and have showed a greater potential for photocatalytic water splitting [46]. Many researchers have synthesized different semiconductor materials using different synthesis roots of having different shapes and sizes. They have reported the effect of porous structure in the synthesized materials on electron diffusion rate for enhanced conversion efficiency for solar cell applications. Researchers have developed significant progress in the creating of innovative substances to use for the photoelectrochemical hydrogen production It was reported that the photoelectrochemical performance of the synthesized materials depends on the rate of generation of photogenerated electron/hole pairs at the electrode[47]. Hayashi et al. had developed solid solutions based upon $(CuGa_{1-y}In_y)_{1-x}Zn_{2x}S_2$(CGIZS) for PEC water splitting. Flux method was employed for the fabrication of powdered CGIZS by using melted salt of LiCl-KCl. Prepared structure possessed single phase structure, micrometer-sized and at 0.6 V of applied potential had showed a photocurrent equals to 4.5 $mAcm^{-2}$ against RHE and had a positive onset potential equals to 1.0V when irradiated with light. Conversion efficiency for solar to hydrogen was of 1.1% attained for PEC water splitting by utilizing two-electrode assembly consisted of photocathode based on CGIZS and photoanode based on $BiVO_4$[48].

Solid thin films are developed in the form of thin layer upon solid support, known as substrate. These are formulated through the condensation of discrete ionic, molecular or atomic species at or near the surface of substrate. Deposition is done either through a physical procedure or a electrochemical/chemical interaction. Thin film deposition mechanism can be designated as the prime technique for the fabrication of various devices This technique has numerous practical applications due to the reliability of this process. Thin films, either amorphous or crystalline, play a critical role in high technology devices. In the field of electronics integrated circuits and solid state devices as well as electronic display devices such as, plasma and fluorescent displays, light-emitting diodes liquid-crystal displays, electrochromic displays and electro luminescent

displays are fabricated using thin film deposition techniques[49]. Apart from these thin film technologies have also find its application in the field of optical coatings, hard surface coatings, space science, defense, photonic, aircrafts, magnetic devices, gas sensor, photoconductors, coating, IR detectors, solar cells, interference filters, temperature regulator in satellite, polarizer's, anticorrosive, superconducting films, decorative coatings and antistatic coatings[50][51]. Thin films has shown better efficiency in photoelectrochemical water splitting due to the distinctive properties of the thickness, geometry and structure of the film[52]. It is examined that material properties drastically alter when converted into thin film. Enhancement in the characteristics of thin films, such as magnetic, optical, wear resistance or electrical, have made these materials beneficial in numerous practical applications[53]. It is because of the fact that physical and chemical behavior of materials is altered at small scale as a result these materials show startling properties, rate of reactivity of materials their strength and conduction ability increase considerably. For instance, gold and platinum show good catalytic behavior at nano scale while they are inert in bulk form[54]. Most of the unique properties of thin films are because of small surface to volume ratio of these materials in comparison to their bulk counterpart which is in turn due to small size. Surface areas of tiny objects are large as compared to their volume. So, their surfaces to volume ratio increases[55]. Semiconductor based thin films which are extensively studied photo electrochemical water splitting are synthesized by employing either physical or chemical deposition[56]. Crystalline metal oxides thin films such as ZnO, TiO_2, SnO_2 and WO_3 with greater porous arrangement have drawn significant interest in the PEC cells to act as a photosensitive electrode[57]. A route for the conduction of electricity; among particles in semiconductors, must be provided to take advantage of their capability through which light energy can be converted to chemical/electrical energy. This can be accomplished through either of methods given below:

Particles from a suspension are applied on a conducting substrate followed by sintering which results in electrical contact among the particles due to charges transport towards the substrate.

Crystalline particles of semiconductor are deposited directly upon the surface of substrate by using chemical or electrochemical pathways.

2.3 Materials Classification:

Extensive work has been performed to develop cost effective and proficient material for hydrogen generation through PEC water splitting Most important parameter of semiconductors for photo water splitting application is its band gap energy (E_g). Band gap energy can be defined as the separation between the energy of conduction band and valance band of semiconductor. Initially electrons are present in valance band but when this material is irradiated with sun light pair of electron hole is generated using the energy of photon of light[58]. These excited photons jump toward conduction band from the valance band of material and these separated electron hole pair are used for redox reactions (Figure 4). As a result the production of hydrogen started at the surface of semiconductor particle due to interaction of separated electron and hole pair with water/adsorbed substrates (e.g., CH_3OH, H_2S)[59].The decomposition reaction of water is possible only if the semiconductor's conduction and valance band potential levels are more negative and positive from the evolution potential of hydrogen and oxygen, respectively. Potential difference equals to 1.23 eV or more than that is required for photocatalytic water splitting to yield hydrogen[60]. It is required that the band gap energy of the material used must be lower as compare to the energy of absorbed photon so that electrons and holes excitation can take place. In general, various semiconductors which had been applied for the photocatalytic splitting of water were active in UV region. For example, anatase type of titanium dioxide (TiO_2) semiconductor which has widespread application due to its good activity[61].Whereas, semiconductors having a low band gap energy which can show excitation upon the absorption of visible light, are very less in number. Such types of semiconductors are investigated and discovered to get the benefits from the plentiful source of visible light which is less energetic.

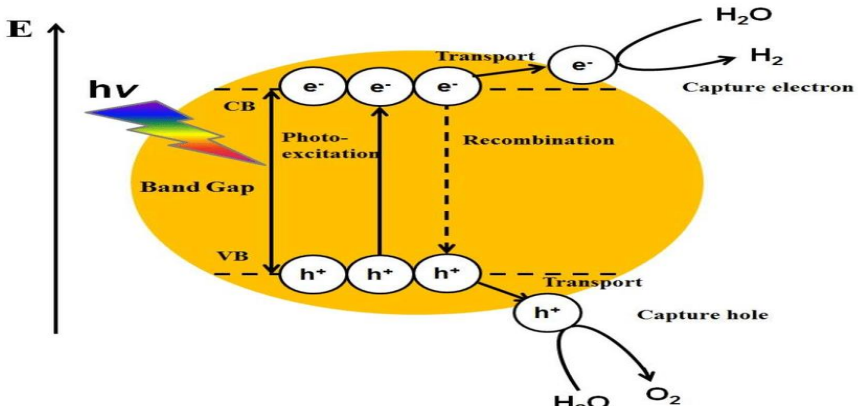

Figure 4 Schematic representation of semiconductor band gap energy structure and the mechanism of electron and hole pairs creation

[reproduced with permission from[62]

Both type of semiconductors either oxides-based or non-oxides based have been experimented for their photodissociation capacity to use in water oxidation reactions. It is because of their capability to absorb photons directly. Non-oxides materials have shown absorption of light in the range of visible region of spectrum. Contrarily, mostly oxides materials are UV active as they show absorption in this region[63]. Major portion of the solar spectrum is consisting of visible light but the benefits of oxide semiconductors are that they are more stable and show high resistivity towards photo corrosion. Transition metals are widely studied for PEC application because of their auspicious durability and electrocatalytic activities.

2.3.1 Semiconductors Non-Oxides:

Metal nitrides possess a number of fascinating properties for example, melting temperature, electronic conductivity and high hardness. Therefore, they have large number of applications in numerous fields. Particularly in reactions like photo, electro or photoelectrocatalytic because of their exceptional electronic structure, good electrical conductance and high corrosion resistance[64]. Nanoporous films of iron nitride (Fe_4N/Fe_3N) were grown upon highly conductive three-dimensional (3D) Ni/graphene foam. The as fabricated material showed robust activity to cat as an electrode for PEC water splitting. It possessed good stability, very small over-potential equals to 238 mV along with current density of 11 mA/cm^2[65]. Xie et al. had developed atomically thin molybdenum nitride (MoN) nanosheets as exceedingly competent

material for the hydrogen evolution applications[66]. Binary and ternary metal oxides are also studied broadly to check their hydrogen production potential through water splitting. These included materials such as defect-rich (MoN), various cobalt nitride Co_4N, Co_3N, Co_2N, (WN), (Ta_3N_5), Ni_3N, (ZrN), (GaN), Ni-Mo-N, Co-Mo-N, Cu-Ni-N, Co_3FeNx, $NiCo_2N$, Fe_2Ni_2N, and Ni_3FeN[67].

Substances synthesized by combining metal semiconductor along with carbon based substances like carbon nanotubes (CNTs) and graphene has noticeably increased the efficiency of PEC devices. These materials as photoelectrodes can effectively reduce the charge recombination; metals act as photo-absorbing substances while CNTs or graphene as a competent charge transporting substance. As a result, the generated charge carriers are effectively separated and transported because of the tremendous conductivity of carbon nano materials. Correspondingly, boosted light captivation and charge carrier formation, enhanced charge separation as well as transference occur[68]. Momeni et al. had synthesized chromium-sensitized TiO_2 nanotubes (CTNT) using bath deposition method with high PEC activity. These materials showed greater light absorption in visible region along with that improved water splitting performance. PEC study was performed in 1M NaOH electrolyte under light irradiation and it was revealed that Cr sensitizing proficiently increased the PEC water splitting efficiency for hydrogen production of the prepared composite[69]. Ismail et al had fabricated the α-Fe_2O_3/CNTs composite by means of spin coating technique. The CNTs were functionalized using –COOH group in three molar nitric acid and distribution of CNTs in dimethyl formamide (DMF)[70].

2.3.2 Semiconductor Metal Oxides:

TiO_2 is important material and is studied extensively for effective PEC water splitting because of its low rate and greater stability, but its efficiency is low because it is UV active as its band gap is 3.03–3.18 eV. Different strategies have been adopted to address this drawback. Kusior et al had established that 3D nanomaterials might be acted as favorable material to develop photoanodes for PEC applications TiO_2 nanoarchitectures were fabricated through the oxidation of titanium foil. In order to develop 1D nanomaterials anodization was carried out inside the electrolyte comprising 1 wt% of ethylene glycol, NH_4F and 2 wt% of water. 3D

flower-like TiO_2 structures were synthesized utilizing chemical oxidation at normal temperature in a 30% solution of H_2O_2. Ultrasonication in acetone as well as in isopropanol was performed to degrease the metal sheets. Apart from this, substrates were also impressed in 35% HCl, washed with deionized water and dried at 100°C in Ar atmosphere. These were anodized electrochemically within a two-electrode assembly of cell in which platinum plate was functioned as cathode and voltage equals to 30 V was provided. Annealing of the devised nanostructures was carried out at 450°C in an inert environment for 3 h. The morphology of both TiO_2 nanotubes 1D and TiO_2 nanoflowers (3D) was different from each other. From XRD analysis it was confirmed that mixture of anatase and rutile form of titania was synthesized. To study the PEC water splitting performance, titania nanoflowers and nanotubes were worked as photoanodes in a characteristic three-electrode design. Response of the dark current was assumed negligible but when semiconductor was illuminated photocurrent increased significantly due to generation of surfeit charge carriers. In the case of 1D nanotubes the maximum value of photocurrent equals to 50.1 μAcm^{-2} was detected in case of sample obtained after anodization for 60 min. Though, flower-like 3D nanostructures display better photocatalytic properties and photocurrent equals to 120 μAcm^{-2} was calculated in this case[71].

Dong et al had reported the synthesis co doped titanium oxide with Ni/Ti^{3+}. For this Zn reduction was carried out of Ni-doped TiO_2 nanotubes under Ar atmosphere. As a result, the band gap of synthesized material was decreased to 2.84 eV. A remarkable conversion efficiency for hydrogen production was achieved i.e. of 1.51%, which was around 10 times greater than that of Ni-doped un-doped TiO_2. It was mainly due to improved light absorption and indorsed separation ability of the photogenerated electron and holes[72]. Hydrogen treatment of TiO_2 nanowires as an easy and economical approach to primarily expand the functioning of TiO_2 nanowires for hydrogen production was studied. Researchers had prepared the hydrogen-treated rutile titanium nanowires (H: TiO_2) in H_2 atmosphere through annealing of pristine TiO_2 upon range of temperature from 200–550 °C. The H: TiO_2 nanowire, at −0.6 V had generated the photocurrent density equals to ∼1.97 mA/cm^2 against Ag/AgCl electrode by using 1 molar solution of aqueous NaOH. Solar-to-hydrogen conversion efficiency equals to ∼1.63% was

achieved through this process[73]. Wang et al had developed heterostructure nano arrays consisted of nanobowls of anatase TiO_2 while nanorods of rutile TiO_2 were grown on its inner surface. These newly developed nano arrays studied for their (PEC) water splitting applications. For the development of heterostructures possessing hierarchical architecture first interfacial lithography of nanosphere was carried out in the next step hydrothermal growth was performed. TiO_2NR@NBarrays offer greater light harvesting capability because of the presence of numerous scattering centers which in turn is due to outspread configuration of rutile nanorods and dimensionally arranged assembly of anatase nanobowls. Connection with the electrolyte was increased due to the large surface area for interaction meanwhile, straight pathways for wild transfer of electron is provided by the nanorods. Furthermore, charge separation was improved due to the anatase/ rutile phase connection in the NR@NB heterostructure. Consequently, the PEC capacities of the TiO_2 NR@NB structures upon the fluorinated tin oxide (FTO) glass substrate had significantly improved. TiO_2 NR@NB photoelectrode produced a photocurrent density equals to 1.24 mA cm^{-2} at the voltage equals to 1.23 V versus reversible hydrogen electrode, which was about two times larger as compare to the TiO_2 nanorods developed directly upon the surface of FTO substrate[74].

ZnO has also shown significant potential for PEC water splitting. Band gap energy of ZnO is equals to ~3.3 eV and possess optoelectronic characteristics alike to TiO_2. Khan et al presented a facile and effective method for fabrication of ZnO and nickel integrated zinc oxide in the form of thin films to develop photoanode for photoelectrochemical water splitting. They used AACVD for the deposition of conductive and highly transparent films Due to incorporation of Ni; the morphology of prepared films altered from bullet like shape to punch like structures, having improved projected surface area for electrochemical activity. Furthermore, incorporation of Ni^{2+}inside host matrix considerably increased its photoelectrochemical functioning by enhancing the rate of charge transport and conductivity. Control over the, crystallinity, carrier mobility, reflectance, charge-carrier density and surface morphology of the developed films had showed significance dependence on the amount of incorporated Ni in ZnO. PEC studies were performed in 1 molar Na_2SO_4 solution as an electrolyte, a Pt wire as a counter electrode, synthesized films as working electrode against Ag/AgCl electrode as a reference

electrode. Under the dark conditions films showed extremely low densities of current. In case of bare ZnO films, at 0.2 V current density was equal to 3.46×10^{-4} A/cm^{-2} while in case of nickel incorporation in ZnO with variable concentrations (15%,10%, 5%, and 2%) photoelectrochemical performance was enhanced. The maximum photocurrent density was calculated in case 15 % Ni which at 0.2 V was equals to 1.7×10^{-3} A/cm^{-2}. The PEC potential was enhanced due to increased active surface, improved conductivity and higher charge transportation[75]. Kant and coworkers described the fabrication of ZnO thin films developed through continuous spray pyrolysis approach and used them as photoanodes for (PEC) water splitting. Furthermore, influence of the applied voltage upon the growth of film and of Al loading (0.02–0.2 wt%) in the Zinc Oxide on optical, morphological, structural, and photoelectrochemical characteristic of synthesized ZnO had been examined. Linear sweep voltammetry studied performed upon the ZnO films g developed on Al doped ZnO seed and along with applied voltage showed a noteworthy elevation in photocurrent density and drop in onset potential when irradiated with light in comparison to the bare ZnO thin films. Dark current was almost negligible for all the prepared samples It was measured that ZnO photoanode yielded the photocurrent density equals to ~19μAcm^{-2} at applied voltage of 0.57V against SCE, that is corresponding to 1.23V (vs. RHE) while photoanode based on ZnO with -0.04 wt% of Al showed a utmost photocurrent density equals to ~182μAcm^{-2} that is considerably greater than ZnO. Photocurrent density showed by other ZnO photoanodes with 0.2, 0.08, 0.06 and 0.02 wt% of Al were equals to 135, 130, 107 and 75μAcm^{-2} respectively. These results depicted that enhancement in the photocurrent is due to the incorporation of (~0.04 wt. %) of Al inside seed layer. It was studied that in when the wt% of Al was either moderate or low in aluminum loaded zin oxide seed layer functioned as a template in the development of ZnO nanostructures and when a percentage of Al was increased, its effect started to appear as a dopant[76].

Fe_2O_3 is known to utilize as a proficient material for electrochemical water splitting. Its band gap is nearly equals to 2.1eV, as a consequence it can absorb almost 40% light of the solar spectrum. It possesses outstanding stability under various aqueous environment as well as is cheap and present in abundant amount. Factors such as synthetic procedure, morphology, size and crystal system play pivotal role in determining PEC efficiency of iron oxide[77]. Kang et

al have prepared anodized iron foams (AFFs) having multidimensional micro/nano - architectures possessed great efficiency as for PEC water splitting as photoelectrode. Fe foams were grown via sintering and freeze-casting. Then anodized electrochemically and employed directly as photoanodes. Remarkable photocurrent density equals to 5mA cm^{-2} was achieved for PEC water splitting using as fabricated iron foams. The anodized Fe foam showed promising results because it possessed supreme characteristics like a high surface area, semiconductor nanostructure confined to low-dimensions, and current collector metal foam having very less electrical resistance. It was anticipated that this method can be employed for the development of photoelectrode using other materials as well efficiency of the fabricated materials can be enhanced by variations in device architecture or through compositional /structural modifications[78].

Kodan et. al. reported the novel heterostructure synthesis of hydrogenated TiO_2/Fe_2O_3 heterostructure. to enhance the photoelectrochemical (PEC) activity of photoanode based on Fe_2O_3 thin-film. This was achieved due to the quicker charge transfer as a consequence of the passivation of surface positions in Fe_2O_3 through TiO_2 overlayer and promising band alignment by means of H_2 annealing of titania overlayer. The valence band offset had been measured via X-ray photoelectron spectroscopy, band gap by optical absorption and work function through Kelvin probe force microscopy to create the diagram of energy band of the established heterostructure photoanodes. The upshift in the band edge position of valence band had confirmed after hydrogen annealing of TiO_2overlayer. In the heterojunction based on Fe_2O_3/H:TiO_2 boosted and well straddled alignment of band edge caused the enhancement in the PEC activity of these in comparison to photoelectrodes comprised of TiO_2/ Fe_2O_3, pristine TiO_2 and Fe_2O_3thin-film. Photocurrent density at applied voltage of 1.23 V was boosted significantly up to 3.36 mA/cm^2 (vs RHE) and having small onset potential equals to 0.1 V when irradiated with light. The detected photocurrent density of as fabricated heterostructure was 15-fold more as compared to bare Fe_2O_3 photoanode. i.e. 0.22 mA/cm^2. It was depicted that how an unpretentious bilayer junction of two structures and its treatment with hydrogen can be applied to augment the PEC potential of grown heterojunctions and provided valued perceptions for the further advancement of other metal oxides heterojunctions[79].

Sn-doped iron oxide nanocorals and nanowires were synthesized and investigated for their PEC water splitting potential as photoanodes. Fe_2O_3 nanowires were made upon a (FTO) glass substrate using hydrothermal route of synthesis, then these were sintered at high temperature in air resulted in the incorporation of Sn, as a dopant which was disseminated from FTO substrate. For the preparation of Sn-doped hematite nanocorals tin (IV) chloride was used as a tin precursor. Photocurrent density equals to 1.86 $mAcm^{-2}$ vs RHE was calculated at applied voltage of 1.23 V which was 1.5 times greater as compare to the nanowires[80].

WO_3 have been also extensively studied for their PEC water splitting applications and have good performance in this regard. Its band gap is nearly equals to 2.45 to 2.65 eV; can capture approximately 12 % of the solar light, reasonable hole diffusion path, cheap and easy preparation methods and fair chemical stability [19]. Fàbrega et al had presented a methodical process for the fabrication of thin films of monoclinic tungsten oxide by applying pulsed laser deposition procedure. A photocurrent density equals to 2.4 $mAcm^{-2}$ was calculated for the prepared films of 18 μm thickness. It was observed from FE-SEM analysis that synthesized WO_3 films were grown through arrangement of organized columns. Notable photocurrent density equals to 3.1 mA cm^{-2} in 0.1 molar solution of H_2SO_4 under the solar illumination was achieved Effectual extraction of holes to electrolyte was detected which was accredited to a likely presence of electrolyte inside the columns of WO_3, even for the films that appears relatively compact. This property along with optical absorption, resulted in the growth of double-stack conformation of WO_3. Faradaic efficiencies achieved without presence of any co-catalyst was above than 50%. In the presence of Al_2O_3 nano layer catalyst faradic efficiency was boosted up to 80% while value of photo current density was sustained[81]. Shen et.al reported that photochemical activity of WO_3 was enhanced effectively by preparing the nano flakes of WO_3 having hierarchical architecture. Hydrothermal route was employed for development of WO_3 nanoflakes, photocurrent density i.e. (1.42 mA cm^{-2}) was boosted 3 times than the pristine tungsten oxide (0.61 mA cm^{-2}). The better photoelectrochemical response could be ascribed to the increased light-harvesting competence provoked by improved interfacial charge transportation at electrolyte-electrode interface and multiple light dispersal characteristics. Exposure to the active sites was enhanced because of the presence of

hierarchical architecture. It was demonstrated that an efficient device for PEC solar energy generation can be developed by employing hierarchical nanostructure as recombination of photogenerated holes and electrons can be reduced. Large quantity of hydrogen was generated upon the surface of Pt because of higher number of availability of electrons. Photogenerated holes participated to oxidize the water in H_2SO_4 electrolyte[82].

$BiVO_4$ has attained substantial attention for water splitting applications owes to its effective absorption capacity as well as band gap energy which ranges for 2.4 to 2.6 eV. It is appropriate material to act as photoanode in PEC water splitting because of its small band gap, refined band edge, and constancy even in acidic solution. Thin films of $BiVO_4$ synthesized via electrostatic spray had shown photocurrent density which was equals to 0.8 $mAcm^{-2}$ upon 1.9 V of an applied potential vs RHE[83]. Khan et.al had reported the hydrothermal approach assisted ultra sonochemically to produce S-$BiVO_4$. H-$BiVO_4$ was also developed for the purpose of comparison using conventional hydrothermal method. SEM analysis of the synthesized S-$BiVO_4$ had depicted that surface consisted of compressed microarrays and possessed quasi flower-liked appearances. Elemental analysis by using EDX had confirmed the presence of O, V and Bi in $BiVO_4$. It was confirmed from the XRD pattern that S-$BiVO_4$ had monoclinic scheelite phase. (FTIR) spectrum presented Bi–V–O and Bi–O vibrational bands at 1630 and 1382 cm^{-1}, respectively. From the diffuse (DRS) value of absorption edge was calculated using DRS studies and was equals to ~515 nm. This value associated with the bandgap value of 2.41 eV that can be employed in PEC water splitting. The photocurrent density obtained from water splitting under light irradiation with simulated visible light source was equal to 50 and 60 μAcm^{-2} for H-$BiVO_4$ and S-$BiVO_4$ respectively. Chronoamperometry measurements were carried out to perform stability test which illustrated that H-$BiVO_4$ was less stable as compare to S-$BiVO_4$[84].

Chapter No. 3

Experimental

3.1 Materials and Methods:

All the manipulations and reactions were performed at room temperature and pressure. Solvents i.e. methanol, ethanol, acetone, pyridine, bi- pyridine, 1-10 phenanthroline were all of analytical grade and used as received from sigma Aldrich without any further purification. Metal salts either metal nitrates or acetates were purchased from sigma Aldrich of analytical grade. For the development of thin films of transition metal oxides, AACVD of respective metal salt solution was performed. The sodium salt of di-ethyl carbamate was synthesized by reacting NaOH with diethyl amine and carbon disulfide (CS_2). In attempt to synthesis the adducts of transition metal diethyldithio carbamate complexes reaction of respective metal salt with sodium diethyldithio carbamate was carried out along with ligands such as pyridine, bi-pyridine and 1-10 phenanthroline.

3.2 Thin Film Deposition of Y_2O_3:

The thin films of yttrium oxide were deposited at the surface of conducting fluorine doped tin oxides (FTO) substrate using AACVD. Firstly, FTO slides were cleaned through bath sonication for 30 min. Detergent solution, ethanol and distilled water were used as solvents for this purpose. The bath sonication was performed for 10 min in each solvent. After the sonication process, FTOs were dried at 110^oC in heating oven. AACVD was performed by using self-made assembly which consist of gas supply, ultrasonic particle generator, connectors and tube furnace as shown in Figure 2. FTO slides were placed in the glass tube and noted their positions; so that ideal deposition point could be identified. Then placed the glass tube of 18mm diameter inside the tube furnace in which FTO substrate were sited. In the next step, (0.53g, 2mmol) of the yttrium acetate hydrate ($Y(CH_3CO_2)_3 \cdot xH_2O$) was added in 20 mL of methanol in a round bottom flask and kept on stirring for 2 hours. This solution was applied as precursor solution to perform the AACVD. Then prepared solution was shifted in a 50mL two necked round bottom

flask which was attached to gas cylinder and to the tube furnace. The flask was placed in an ultrasonic nebulizer. The argon gas was passed through the system and after that, tube furnace was turned on and the temperature was raised up to 450°C. After desired temperature limit was reached atomizer was switched on and the generated aerosol was carried towards the reaction tube through argon gas flow with pressure of 120 mL/min. Aerosol was generated through humidifier and was carried on the heated substrate by using inert carrier gas. Deposition was completed for yttrium acetate in 120 mins.

3.3 Thin Film Deposition of Fe_2O_3:

The same procedure was followed for the deposition of iron oxide thin films except the amount of precursor salt i.e. iron acetate. In this case solution of Iron acetate (0 46g, 2mmol) in 20 mL of methanol was employed as precursor solution and gas flow was kept 120 mL/min. Film deposition temperature was kept at 420°C and deposition was completed in 75 min

3.4 Thin Film Deposition of CrO_3:

For the fabrication of chromium oxide thin films using AACVD, chromium nitrate nona hydrate (0.8g, 2mmol) was dissolved in 20 mL of CH_3OH and was utilized as precursor solution. Inert carrier gas flow rate in this case was 90 mL/min while temperature for deposition was equal to 400°C and completion time was 90 mins. Fabrication of thin films was carried out by following the same procedure as for Y_2O_3.

3.5 Other Attempted Reactions for the Synthesis of Metal Complexes:

We performed a series of resections to synthesis the transition metal diethyldithio carbamate complexes. These can be used as a single sources for the fabrication of metal sulfides thin films using AACVD.

3.5.1 Synthesis of $Na(C_2H_5)_2NCS_2$:

The desired compound was prepared according to the literature procedure[85]. Firstly, solution of 4g of sodium hydroxide (NaOH) was made in 40 mL of water and its temperature was drop down to ~ 4°C by keeping in the ice bath. $(CH_3)_2NH$ equals to (7.3g,10mL) was added to this solution. 10 mL of Carbon disulfide (CS_2) in 40 mL of ethanol was added dropwise to the mixture of NaOH and $[(CH_3)_2NH]$ while the temperature was sustained from 4 to 8°C. A light-

yellow colored mixture was obtained upon the complete addition of CS_2 for almost 90 mins. The mixture was stirred for further 15 mins. Then 100 mL of methanol was added to this mixture. This mixture was kept at room temperature in fume hood for 3 days. Needle like light yellow colored crystals of $Na(S_2CNEt_2)$ i.e. Na(dtc) was obtained upon slow evaporation which was washed 3 times with cold methanol. And then stored in a cleaned glass vial in vacuum desiccator for future use. Its melting point was 80°C.

3.5.2 Synthesis of $(C_2H_5)_2NH_2(C_2H_5)_2NCS_2$

50% HCl was added dropwise in (2g, 3mL) of $(CH_3)_2NH$ in a round bottom 50 mL flask until the pH dropdown to 1. Shifted the mixture in flask and evaporated it using rotary evaporator. A white ppt was obtained which was dried in oven and then dissolved in methanol. The obtained clear solution was added dropwise in a flask containing solution of Na(dtc) in methanol. The reaction mixture was stirrer with magnetic stirrer for 2 hr. after the stirring, the solution was evaporated in rotary evaporator. A solid mass was obtained from which sodium chloride was precipitated out upon addition of CH_3CN. On evaporation of solvent from the filtrate, $(C_2H_5)_2NH_2(C_2H_5)_2NCS_2$ was prepared. The obtained $(C_2H_5)_2NH_2$(dtc)was used in the following reactions.

3.5.3 General Procedure for Synthesis of Metal dithiocarbamate:

Adducts of metal carbamate complexes – $M(dtc)_3L_n$ where M= Gd, Eu, Ga, Y, Cr and n=1 L= pyridine, n=2 L=bipyridine and n=3 L =1,10 phenanthroline were synthesized by reaction of respective N(dtc) where N=Na or $(C_2H_5)_2NH_2$ with metal salts. Different solvent like methanol, acetone, acetonitrile or water were used for the synthesis of metal complexes. We have reacted synthesized sodium or diethylammonium dithiocarbamate with respective metal salt in 3:1 ratio. The reaction mixture was kept on stirring for almost 4 hours. Precipitate (ppts) was formed that was separated out through filtration. The filtrate was dried to obtain crystal of the respective metal complexes. Unfortunately, no crystal was obtained rather than a slurry mixture or gel-type product was obtained at the end of all reactions. The obtained precipitates in all reactions were tried to dissolve in different solvent but was not successful. This indicated that metal complexation was not occurred.

3.5.4 Synthesis of $Gd(dtc)_3L_1$:

In a round bottom flask, (1.8g,4 mmol) of Gd $(NO_3)_3.6H_2O$ was added into 10 mL of CH_3OH. Furthermore, (2.1g,12 mmol) of Na(dtc) in 50 mL CH_3OH was added dropwise in the above solution. The reaction mixture was stirred on hot plate to result a precipitate settled at the bottom of the flask; washed, filtered and checked for its solubility in the different solvents i.e. hexane, , dichloromethane, acetone , chloroform, methanol, ethyl acetate, ethanol, water and acetonitrile. The precipitate was insoluble. Energy dispersive x-ray spectroscopic (EDS) analysis of the precipitate was performed as shown in Figure 5. In the filtrate obtained from the reaction mixture, 40 mL of pyridine was added and placed for crystallization at room temperature. No crystal was obtained instead a residue of polymeric gel was remained at the bottom of beaker. In this residue, we added 40 mL of tetrahydrofuran which resulted in the appearance of a water soluble ppts of white color ($NaNO_3$); separated. The solvent was evaporated, then ppt was washed 3 times with 60 mL of ethyl acetate and 50mL of water to separate organic phase and was dried by adding 12g of anhydrous sodium sulphate in this organic phase. The solvent was evaporated in rotary evaporator and when 5 mL of solvent was remained- kept it for crystallization, again no crystals was formed. Then added 5 mL of acetone and after mild heating when ~ 1.2 mL remained kept it in refrigerator in air tight vial for 30 days but no crystals were grown.

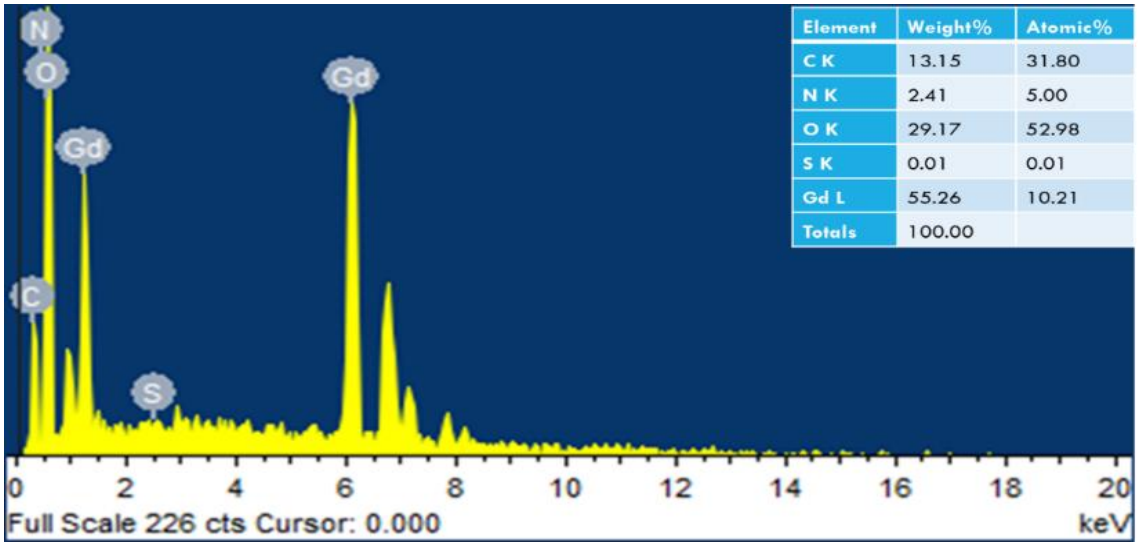

Figure 5 EDS spectrum of the powder obtained from reaction of Gd $(dtc)_3L1$.

3.5.5 Synthesis of Gd $(dtc)_3L_2$:

For the synthesis of Gd $(dtc)_3L2$, solution of (1g, 2mmol) (Gd $(NO_3)_3.6H_2O$) in 10 mL of CH_3OH was added to the solution (1.14g,6mmol) of Na(dtc) and (0.34g, 2mmol) of bipyridine in 40 mL of methanol. Stirring was continued for 4 hours. The precipitates were checked for solubility in various solvents but was insoluble. EDS analysis of the powder is shown in Figure 6.

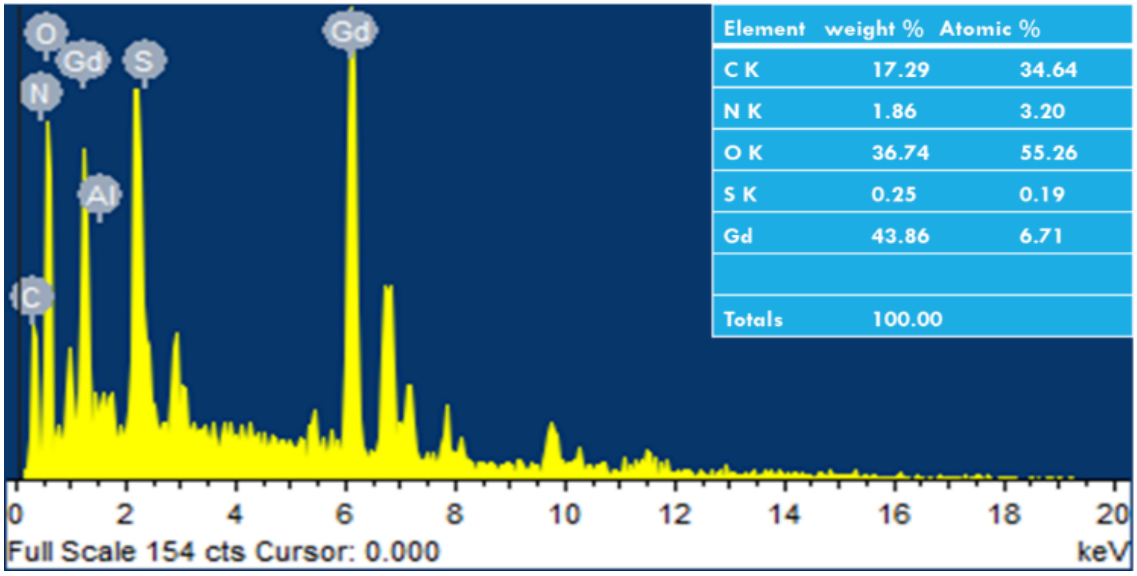

Figure 6 EDS spectrum of the powder obtained from reaction of Gd $(dtc)_3L2$

Yellowish brown filtrate was kept on hot plate at 40°C for 30 minutes. After that placed it in ice bath for 2 hours. It was solidified. Dissolve the solid material in minimum amount of acetone and placed it in air tight vial and kept in refrigerator for 7 days to crystalize it. After 7 days brownish colored polymeric mass was obtained but no crystals were grown. Performed EDS of the product as shown in Figure 7.

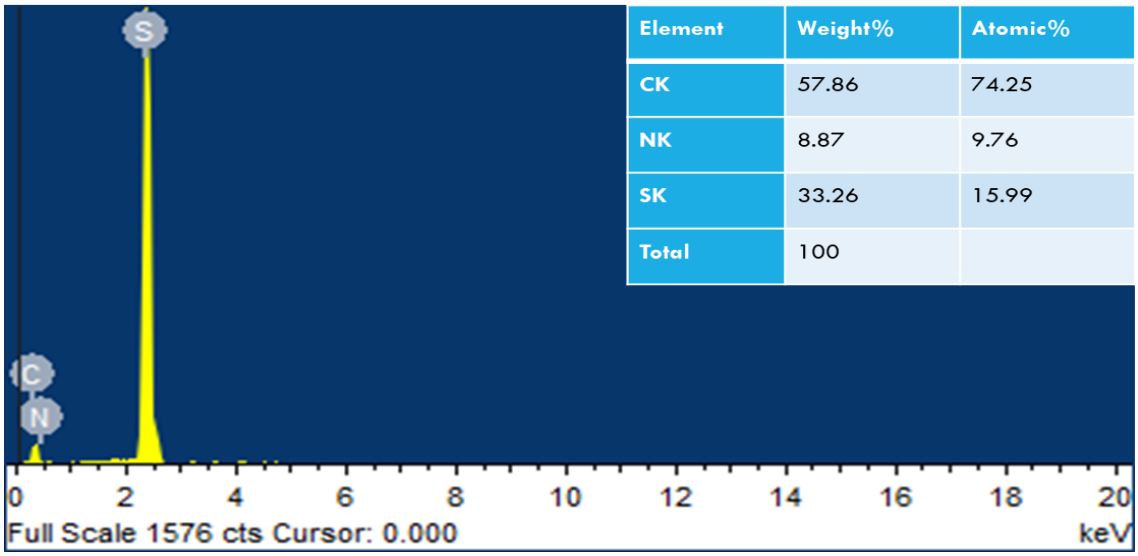

Element	Weight%	Atomic%
CK	57.86	74.25
NK	8.87	9.76
SK	33.26	15.99
Total	100	

Figure 7 EDS spectrum of the filtrate after concentration from reaction of Gd $(dtc)_3L2$

3.5.6 Synthesis of $Gd(dtc)_3L_3$:

3.5.6.1 Synthesis of $Gd(dtc)_3L_3$using Na(dtc)

In first attempt we dissolved (0.45g,1mmol) of Gd $(NO_3)_3.6H_2O$ and (0.513g, 3mmol) of Na(dtc) in 5mL and 20 mL of 1:5 of CH_3OH:CH_3CN. Solution of (0.18g, 1mmol) of 1,10-phenanthroline was made in 5mL of CH_3CN. After 15 mins of stirring white ppts appeared. Stirring was continued and ppts was dissolved. As a result of further stirring for almost 4 hours no ppts appeared. Kept this in refrigerator for 24 hours no ppts appeared. Evaporated the solvent in rotary evaporator. Solid powder was obtained. It was partially dissolved in acetonitrile; the un-dissolved powder was separated through filtration. Filtrate was kept for crystallization. Performed the EDS of powder. Figure 8(a)

In the second attempt we used water as solvent. In distilled water (5mL) made the solution of Gd $(NO_3)_3.6H_2O$ (0.25g, 0.5mmol). To this added the solution of (0.1 g, 0.5mmol) of 1,10 phenanthroline (1.1g, 6mmol) of $Na(S_2CNEt_2)$ and stirred for 4 hours. White colored ppt was obtained which was insoluble in acetone, ethanol, dichloromethane, methanol, carbon disulfide, and 8:2 of methanol and acetonitrile.

3.5.6.2 Synthesis of $Gd(dtc)_3L_3$using $(C_2H_5)_2NH_2(dtc)$

Exactly followed the procedure mentioned in the literature[86] to synthesize the $Gd(S_2CNEt_2)_3$. When the solutions of and Gd $(NO_3)_3.6H_2O$ (0.45g,1mmol) in 5mL acetonitrile was mixed with solution of $(C_2H_5)_2NH_2$ (dtc) (0.68g, 3mmol) and (0.18,1mmol) of 1,10- phenanthroline was mixed light pinkish colored powder was formed. That powder was not soluble in any of the solvents. Performed the EDS of powder as shown in Figure 8(b).

Performed the TLC of the filtrate and compared it with the TLC of solution of 1,10 phenanthroline to confirm the completion of reaction. After that kept the filtrate for crystallization. After complete evaporation of solvent, EDS of obtained material was performed as shown in Figure 9.

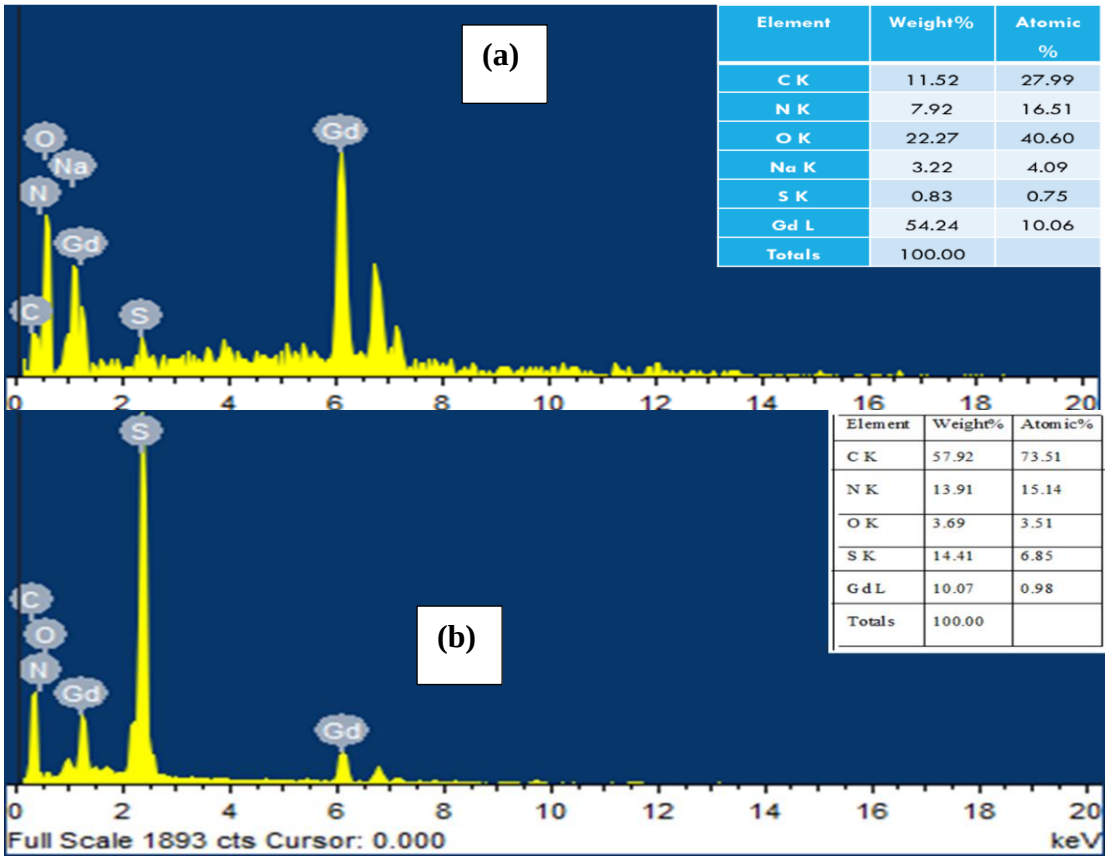

Element	Weight%	Atomic %
C K	11.52	27.99
N K	7.92	16.51
O K	22.27	40.60
Na K	3.22	4.09
S K	0.83	0.75
Gd L	54.24	10.06
Totals	100.00	

Element	Weight%	Atomic%
C K	57.92	73.51
N K	13.91	15.14
O K	3.69	3.51
S K	14.41	6.85
Gd L	10.07	0.98
Totals	100.00	

Figure 8 EDS spectrum of the powder from reaction of Gd $(dtc)_3$L3(a) with Na(dtc) (b) with C_2H_5NH (dtc)

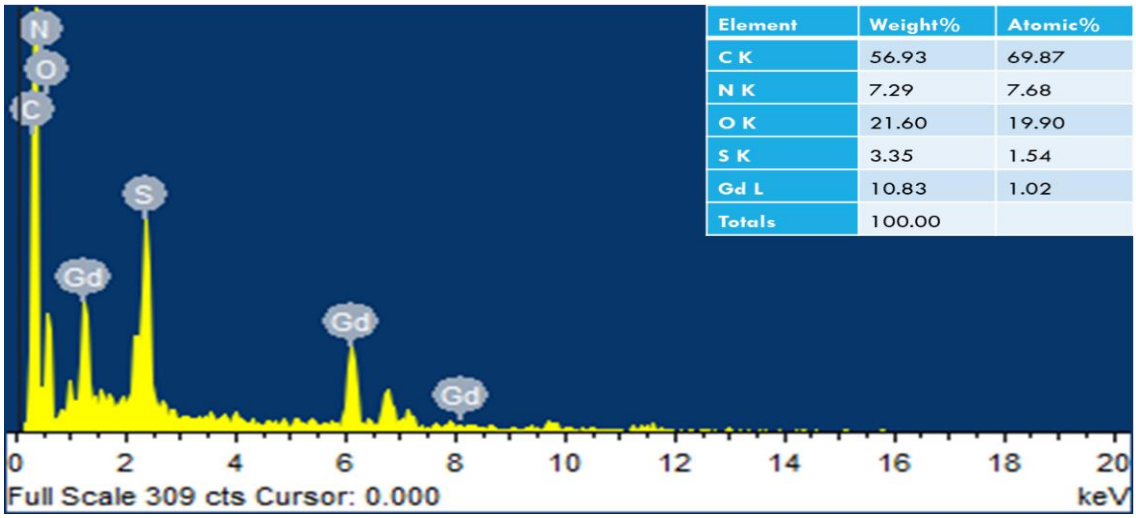

Element	Weight%	Atomic%
C K	56.93	69.87
N K	7.29	7.68
O K	21.60	19.90
S K	3.35	1.54
Gd L	10.83	1.02
Totals	100.00	

Figure 9 EDS spectrum of filtrate after concentration from reaction of Gd $(dtc)_3$L3

3.5.7 Synthesis of $Eu(dtc)_3L_2$:

Solution of Na(dtc) (0.5g, 3mmol) and (0.15g, 1mmol) of bipyridine in 15 mL of methanol was added to solution of europium nitrate pentahydrate (0.42g,1mmol) in methanol (5 mL) and stirred for 8 hours. Evaporated the filtrate at mild heating when half of the mixture was remained kept it in ice bath for crystallization for 24 hours. No crystals appeared. Kept this mixture at room temperature after slow evaporation jell like materials was obtained but no crystals were grown, performed the EDS of as shown in Figure 10. Solubility of powder was checked in different solvents but it was not soluble in any.

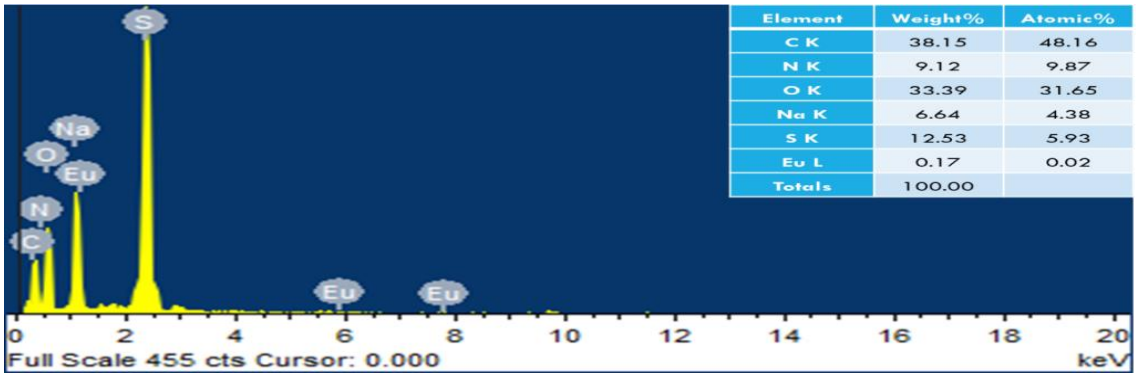

Element	Weight%	Atomic%
C K	38.15	48.16
N K	9.12	9.87
O K	33.39	31.65
Na K	6.64	4.38
S K	12.53	5.93
Eu L	0.17	0.02
Totals	100.00	

Figure 10 EDS spectrum of the filtrate after concentration from reaction of $Eu(dtc)_3$

3.5.8 Synthesis of $Ga(dtc)_3L_1$:

Solutions of (0.25 g, 1mmol) of gallium nitrate and (0.5g, 3mmol) of Na(dtc) in 10mL and 30mL of C_3H_6O were mixed through stirring. Color was changed from light yellow to milky white. After complete addition, stirring was continued for further 10 min precipitates appeared. Upon filtration bright yellow filtrate was obtained in which 30 mL of C_5H_5N was added and kept in fume hood at room temperature for crystallization. After 7 days, polymeric mass was formed. Performed the EDS of both filtrate and residue as shown in Figure 11 and 12.

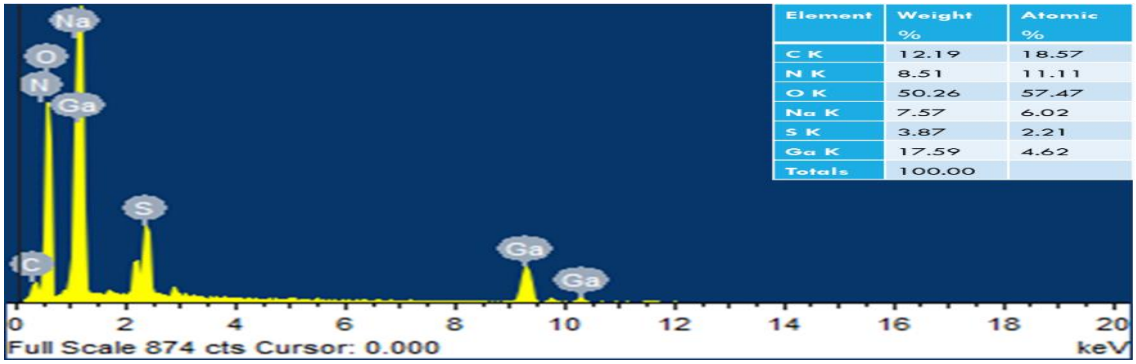

Element	Weight %	Atomic %
C K	12.19	18.57
N K	8.51	11.11
O K	50.26	57.47
Na K	7.57	6.02
S K	3.87	2.21
Ga K	17.59	4.62
Totals	100.00	

Figure 11 EDS spectrum of powder from reaction of $Ga(dtc)_3L1$.

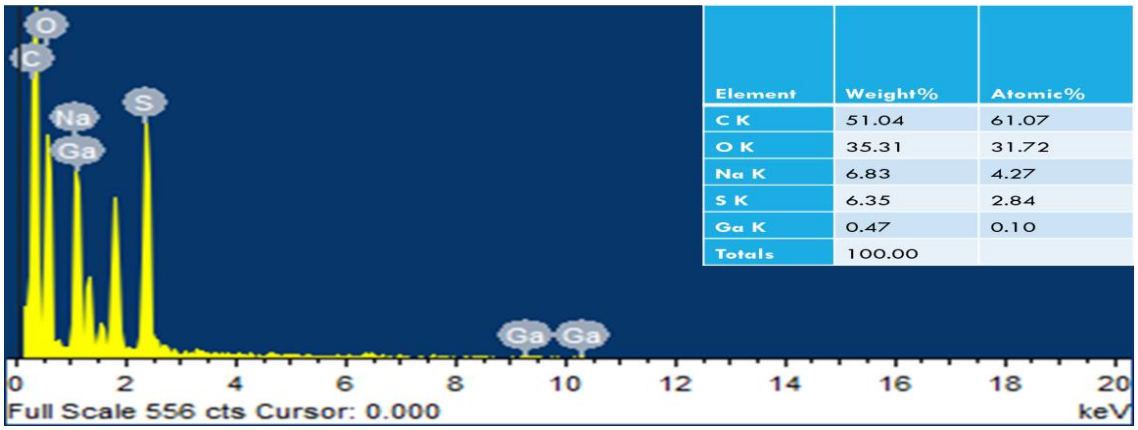

Element	Weight%	Atomic%
C K	51.04	61.07
O K	35.31	31.72
Na K	6.83	4.27
S K	6.35	2.84
Ga K	0.47	0.10
Totals	100.00	

Figure 12 EDS spectrum of filtrate after concentration from reaction of $Ga(dtc)_3L1$

3.5.9 Synthesis of $Y(dtc)_3$:

In first attempt dissolved (0.5g,1.8mmol) and (0.96g,5.4mmol) of yttrium acetate and Na(dtc) in 50mL and 30 mL of CH_3OH, respectively. These two solutions were mixed and stirred overnight. Precipitate appeared which was collected through filtration and dried in oven. Performed the EDS of the precipitates as shown in Figure 13.

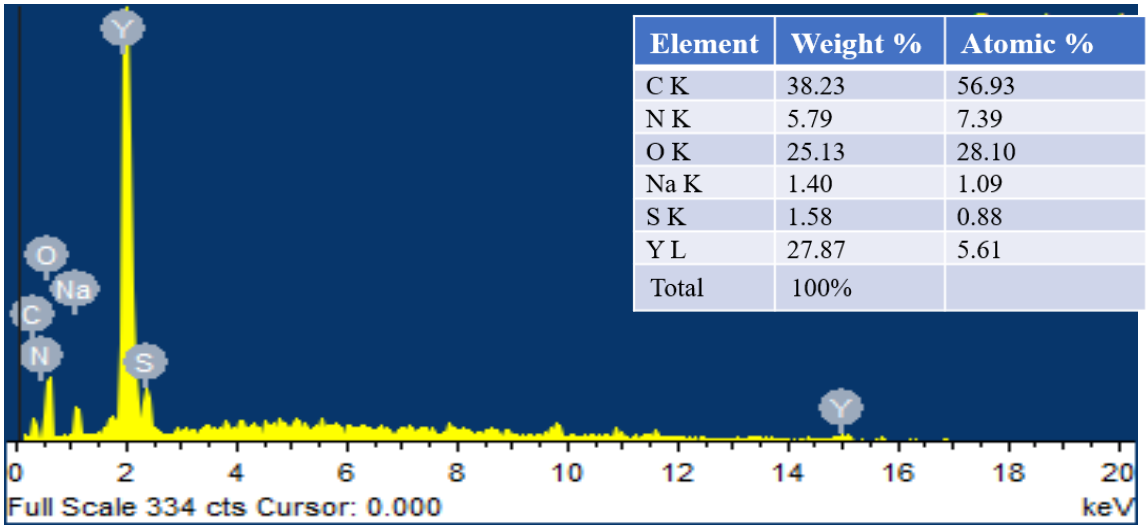

Element	Weight %	Atomic %
C K	38.23	56.93
N K	5.79	7.39
O K	25.13	28.10
Na K	1.40	1.09
S K	1.58	0.88
Y L	27.87	5.61
Total	100%	

Figure 13 EDS spectrum of the powder from reaction of $Y(dtc)_3$

In second attempt instead of CH_3OH, solutions were prepared in distilled water and the amount of Na(dtc) was 3 equivalents i.e. (2.8g, 16mmol). Repeated the same steps as in above mentioned reaction. White colored powder precipitated out. Noted the M.P of powder it decomposes at 162°C. Checked its solubility in various solvents $CHCl_3$, dimethyl sulfoxide, CH_3OH, C_2H_5OH, C_3H_6O, CH_2Cl_2, CS_2 and in 8:2 of CH_3OH and C_5H_5N but it was insoluble in all.

In the third attempt we tried to grow crystals by adding pyridine ligand. First dissolved (0.5g,1.8mmol) of yttrium acetate and 3 equivalents i.e. (2.8g, 16mmol) of Na(dtc) in 30 mL and 40 mL of methanol respectively. Mixed these two solutions and stirred for 24 hours after that added 20 mL of pyridine ppts formed. Separated those via filtration and kept the filtrate for crystallization. No crystals grow in 4 days then kept it in refrigerator again no crystals formed.

After that added 15 mL of acetone and kept in refrigerator for 4-hour ppts appeared. Ppts was separated out. Those ppts were of sodium acetate.

3.5.10 Synthesis of $Cr(dtc)_3$:

Took (0.25g, 6mmol) of chromium nitrate hydrate and three equivalents (0.96g, 5.4mmol) of Na(dtc) and made their solutions in 5mL and 20 mL of distilled water. Mixed these two solutions through stirring after 30 min ppt was formed. Stirring was continued for further 2 hours. After that filtrated it and collected the powder which was insoluble in various solvents.

3.6 Possible Reasons for the Unsuccessful Reactions:

We have performed the EDX analysis of either obtained filtrate or precipitate or both for the number of aforementioned unsuccessful reactions. Most of the time, we found that the EDX analysis of the filtrate did not contain the metal element. Whereas, the precipitate had the appropriate percentage of metal element but amount of sulfur in it was negligible. It was estimated that the metal complexation did not occur. We tried number of possible variations, but outcome was almost same every time. The possible reasons which caused the reactions not to accomplish successfully can be as follows.

Un-availability of Dry Conditions and Glassware:

These reactions are expected to perform under controlled environment using vacuum line and schlenk apparatus. Since, we do not have this facility in the lab which might be the reason of un successful reactions.

Occurrence of Chugaev Reaction:

The other reason might be the occurrence of chugaev reaction which is typically expected at high temperature but because of higher metal atomic number it may be proceed at room temperature. During Chugaev reaction alkene is produced through intermolecular elimination

Mechanism of the process is given

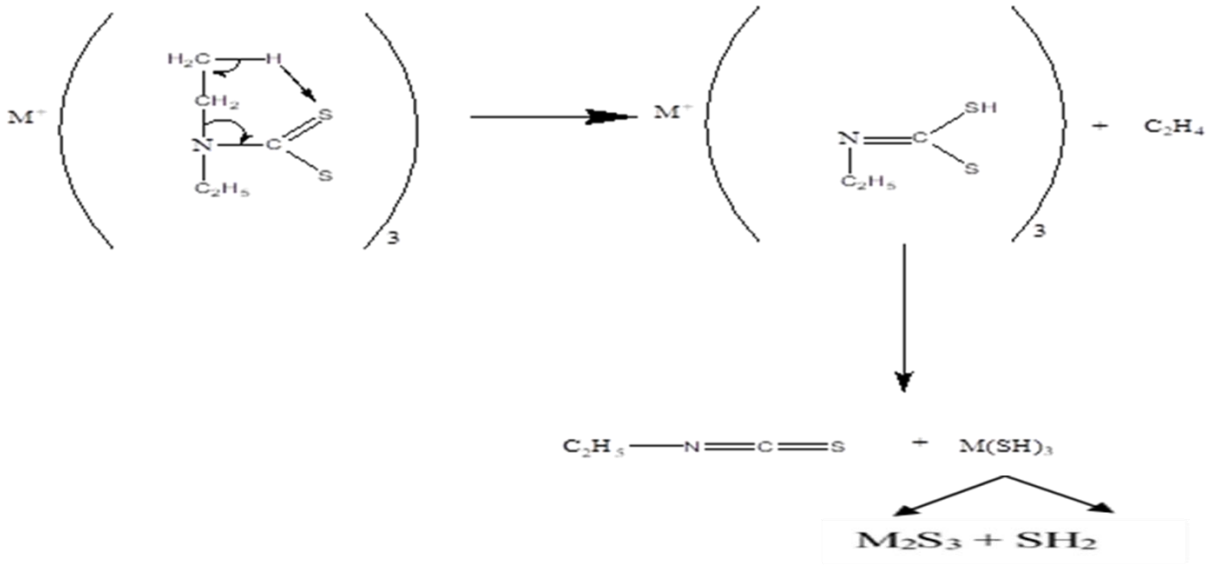

In the first step hydrogen will remove from carbon atom present at β position to the nitrogen of carbamate in a syn-elimination and resulted in the elimination of ethene.

In the next step product will decompose to yield metal sulfide as sulfides are un-stable, they will convert into metal oxides. From EDS results it is clear that significant amount of oxygen and metal present in precipitated out product.

Un-availability of Higher Number of Amine:

These reactions might be carried out successfully if higher number of amine is employed in synthesis of carbamate as it is reported that these higher number amine groups are more suitable to form complexes. We were limited in supply to use higher number amine groups because of their unavailability. Therefore, this also hinder the success of the aforementioned reactions.

3.7 Characterization of Prepared Thin Films:

Once the thin films were synthesized, they were characterized to check phase, purity, surface morphology and optical properties, using the following techniques such as X-ray diffraction(XRD), fourier transform infrared spectroscopy(FTIR), field emission scanning electron microscopy (FESEM), and diffuse reflectance spectroscopy (DRS). These techniques are discussed briefly here.

3.7.1 X-Ray Diffraction:

(XRD) is one of non-destructive tool used to study the crystal structure of given material, it demonstrates the arrangement of atoms within a unit cell. Diverse diffraction patterns are generated depending upon the different arrangement of atoms X-Rays are produced through cathode tube, filtered to generate monochromatic radiation.

Constructive interference results when Bragg's law is satisfied. Incident X-rays scanned the sample over a range of angle θ, known as Bragg's angle. Bragg's law can be written in the form of equation as

$$2d\ sin\theta = n\lambda \qquad (5)$$

Where, d donates the inter spacing between the planes, θ is the angle among incident ray and reflecting crystallographic planes, n is integer, and λ is the wavelength in nm of incident rays. So, according to this law for constructive interference to occur it is necessary value of 2d sinθ should equal to the integral multiple of wavelength. Usually, X-ray wavelength λ has constant value in most of the diffractometers. Bragg's law gives the angle at which diffraction peak is produced via constructive interference of X-rays which are scattered by interaction with the equivalent planes of atoms. These peaks are linked with the planes in the crystal. Each family of planes gives a diffraction peak at a distinctive angle 2θ only. Miller indices (hkl) are employed to categorize diverse planes of atoms and helps to analyze the atomic structure of sample. Shape of peaks give information about crystallinity. Broad peaks are for amorphous and sharp peaks are for crystalline structures. Crystalline size can be calculated using a Scherrer formula which is as follows

$$\text{Crystallite size} \qquad Dp = \frac{K\lambda}{(B\cos\theta)}$$

where: Dp is equal to average crystallite size, K is Scherrer constant whose value alters from 0.68 to 2.08(To calculate the crystalline size, we took value of K equals to 0.94), λ is wavelength of X-rays, B is full width half maximum of the observed peak, θ position is XRD peak which is half of 2θ. The XRD patterns of the samples were obtained in the range 20^o to 80^o using a diffractometer with Cu-Ka radiation (k = 1.5406 Å) at room temperature. Results are given in chapter 4.

3.7.2 Fourier Transform Infrared Spectroscopy:

Fourier Transform Infrared Spectroscopy (FTIR)was employed for the detection of different functional groups. Every region is associated with specific functional group and the peaks shown in this region confirming the presence of that functional group in the analyzed material. In this infrared light is irradiated upon the sample. When these radiations interact with the molecules of targeted material; some amount of radiation is absorbed and measured. As a results excitation took place from ground state to excited state. From the absorbed wavelength the energy among the ground sate and excited state can be estimated as this wavelength a is directly linked to energy difference between two states. Every wavelength is associated with the specific functional group which are present in the molecular structure. Metal oxygen bond les in the range of near IR i.e. from 780 nm to 2500 nm. Typically, below 1000nm. IR plot that is generated on screen contains absorbance or %transmittance along y-axis while wave number on x-axis. FTIR analysis with model FT/IR-6600 type A was performed to identify the presence of metal oxygen bond in the thin films of desired transition metal oxides.

3.7.3 Diffuse Reflectance Spectroscopy:

Diffuse reflectance is an optical procedure usually used in UV-visible or infrared regions to attain data of molecular spectroscopic. It is normally used to obtain the spectra of thin films or powdered sample and require very less sample preparation. Electromagnetic radiations which are reflected from the surface are analyzed to get a reflectance spectrum. These radiations are assembled as a function of wavelength (nm) or frequency (wavenumbers cm^{-1}). Two types of reflections can be detected, diffuse reflection and regular or specular reflection. The specular reflection is related with the reflection from smooth or polished surfaces such as mirrors while diffuse reflection is linked with reflection from rough or dull surfaces such as powders. In diffuse reflectance, the angle of reflection from the sample, of incident radiation is independent of the angle of incident. After the radiation interaction with the sample, a combination of diffraction, reflection, absorption, or refraction and absorption of incident beam takes place.

The above phenomena are described by various theories but the usually used theory to explain the diffuse reflectance spectra is the theory of Kubelka-Munk which is donated as:

$$F(R) = \frac{(1-R)^2}{2R}$$

Where F(R) is equals to the Kubelka-Munk function alike to extinction coefficient α and R depicts the reflectance. This can be used to obtain the direct band gap of the sample by multiplying the energy (eV) with the co-efficient and is given as

$$E_g = [\mathrm{F(R)} \times \mathrm{h\upsilon}]^2$$

Where exponent *n* is equals to 2 in case of direct band gap transitions and for indirect transitions it is equals to 0.5. UV–visible spectroscopy was run employing diffuse reflectance mode. For this, lymbda 950 UV–vis-NIR spectrophotometer was used.

3.7.4 Scanning Electron Microscopy:

In scanning electron microscopy (SEM), fast moving electrons are bombarded upon the surface which interact with the atoms of the surface of material. This interaction among the surface of sample and electron are used to obtain the information about surface morphology, topology and composition of the product. of sample gives the information about topology, morphology and composition of sample. In SEM, source for electrons is consisted of tungsten, because of its and low vapor pressure and low cost. Electrons are emitted via electron gun which is coupled with cathode. The whole set up functioned in the presence of high vacuum. Following the electron gun, couple of condenser lenses are fitted which are used to focus the electrons over the area ranges from 0.4nm to 5nm in diameter. Next, deflected plates are present that functions to scatter the electrons beam and these scattered electrons scan the targeted area of material. Due to the interaction among electron and sample energy is exchanged between these. This energy exchange results in the emission of electromagnetic radiations, back scattered and secondary electrons. The produced signals are sensed by distinctive detectors and the sample image is developed and displayed on the screen of computer. Scanning electron microscopy (SEM) was used to study the surface morphology of the thin film.

3.7.5 Energy Dispersive X-ray:

EDX/EDS is a promising method which was used to identify the elemental composition of a material. It is generally coupled with SEM or TEM. Bombardment of high energy beam upon an atom results in the elastic and inelastic collations among the electronic cloud and incident beam, which may cause the knockout of inner electrons. Higher state electrons will move to fill up these vacancies and as a result characteristic X-rays are emitted. Two types of sources are utilized in EDX i.e. X-rays and electronic beam X-ray source is used in XRF while electron beam is employed in SEM or TEM. In EDX detector upcoming X-rays are detected via a sensor, the energy of these X-rays is converted into a voltage through a preamplifier, finally these signals can be measured via a pulse processor and send to computer for further analysis and display. EDS analysis was performed to check elemental composition of the samples obtained from attempted reactions to synthesize metal complexes as shown in the synthesis section.

Chapter No. 4

Results and discussion

4.1 Phase Identification:

The XRD patterns of the samples were obtained in the range 20^o to 80^o using a diffractometer with Cu-Ka radiation (k = 1.5406 Å) at room temperature.

4.1.1 Iron Oxide:

Sharp peaks are present in the in the X-ray diffractogram which indicates that the prepared films consist of crystalline structure. Peaks present at the 24.31, 33.32 and 35.79 2θ position which attributed to the (012), (104) and (110) rhombohedral crystal orientation. These values are perfectly matched with the (JCPDS) reference number 00-001-1053 of the hematite (Fe_2O_3) structure. These films possessed rhombohedral crystal system, space group R-3c and 167 Space group number. Peaks present at the 2θ position of 31.86 and 66.36 are of SnO, as films are deposited upon FTO coated glass substrate. Average crystallite size for Fe_2O_3 thin films calculated by using Scherrer formula is equals to 122.24 nm. (Table 1)

Table 1 Calculation of average crystallite size of as fabricated Fe_2O_3 thin films upon FTO substrate using AACVD at 420°C

Peak position 2θ (°)	**FWHM B_{size} (°)**	**Dp (nm)**	**Dp Average (nm)**
24.3142	0.1181	71.92	**122.24**
33.3211	0.059	146.91	
35.7913	0.059	147.90	

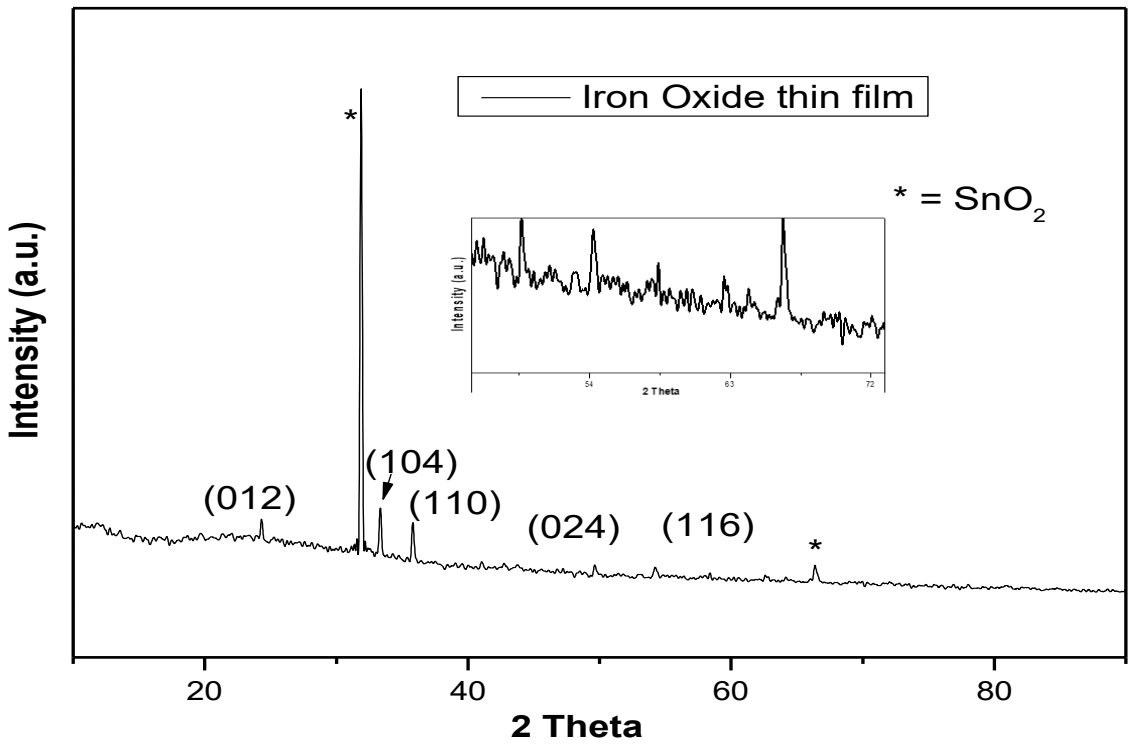

Figure 14 (a) XRD peak pattern of as fabricated of Fe_2O_3 thin films on FTO substrate using AACVD at 420°C

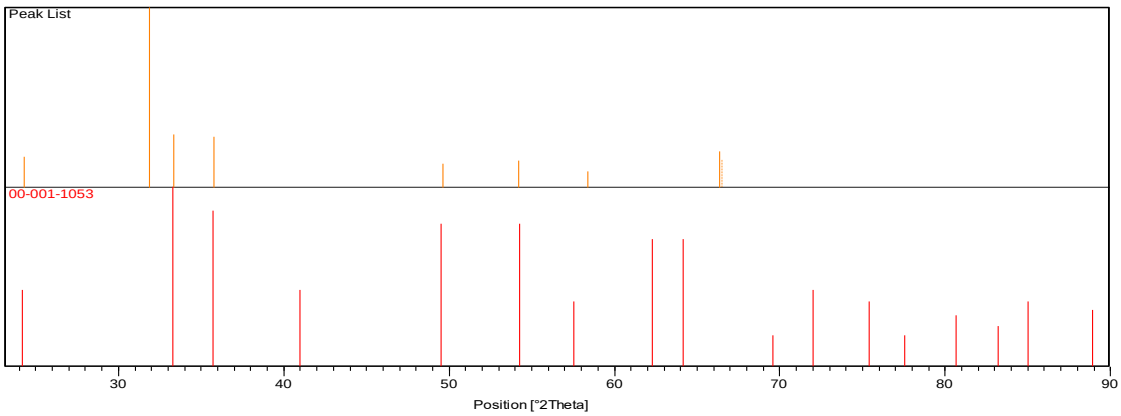

Figure 14 (b) Matching of peaks with reference pattern for Fe_2O_3

4.1.2 Yttrium Oxide:

Sharp peaks present at 2θ position of 32.2, 38.1, 44.0,52.8, 62.077, 64.2, 66.0 and 79.7 are corresponding to (400), (420), (431), (600), (543), (640), (721), and (820) is of cubic crystalline orientation of yttria(Y_2O_3) films. It is in accordance with the JCPDS cards reference number 00-041-1105. The remaining peaks are attributed to fluorinated tin oxide. Average crystallite size obtained from XRD data using Scherrer formula is equals to 106.89nm. (Table 2)

Table 2 Calculation of average crystallite size of as fabricated Y_2O_3 thin films upon FTO substrate using AACVD at 450°C

Peak position 2θ (°)	**FWHM B_{size} (°)**	**Dp (nm)**	**Dp Average (nm)**
38.129	0.072	55.82	**106.89**
44.024	0.048	128.26	
51.899	0.072	136.59	

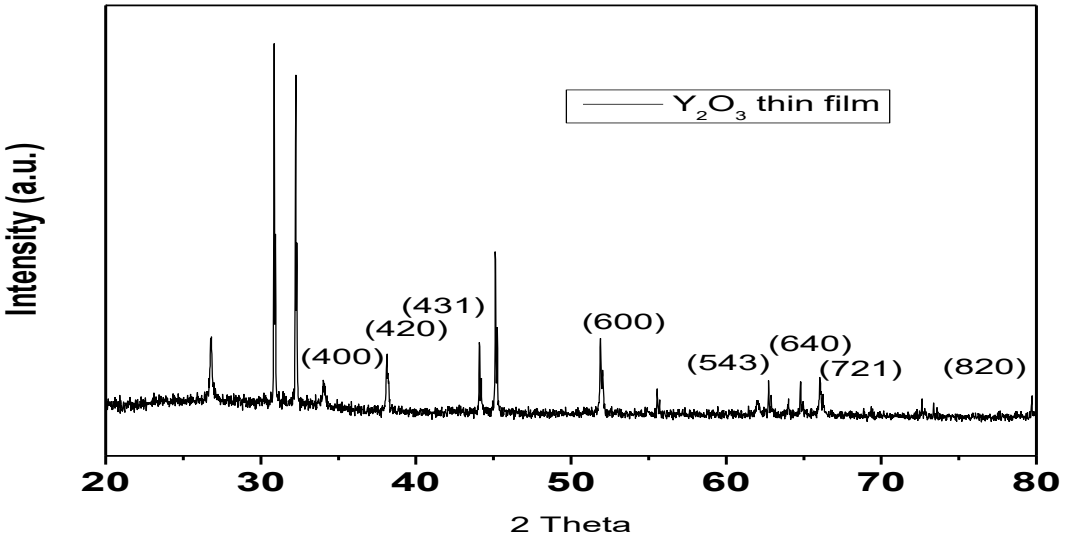

Figure 15 (a) XRD peak pattern of the as-fabricated Y_2O_3thin film on the FTO substrate using AACVD at 450ºC.

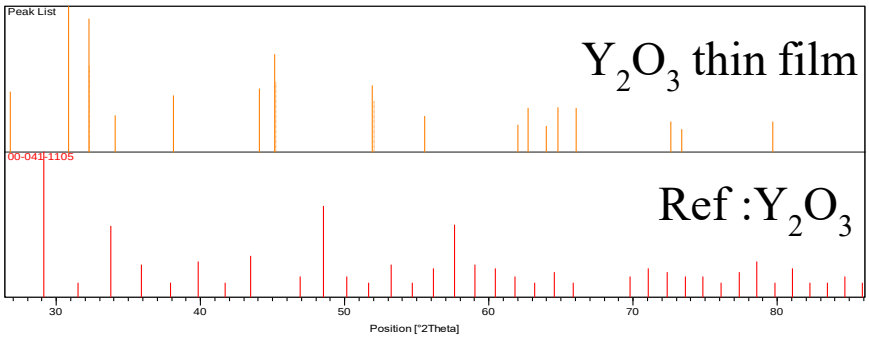

Figure 15 (b) Matching of peaks with reference pattren for Y_2O_3

4.1.3 Chromium Oxide:

Peaks present at the 38.1,52.7, 54.58, 61.79 and 66.62 2θ position matched with the JCPDS card reference number 00-001-0622 for chromium oxide (CrO_3). These peaks correspond to (211), (311), (222), (250) and (332) reflections of orthorhombic crystalline structure.

Remaining peaks are corresponding to tin oxide. Average crystallite size obtained is 53.04nm as shown in table 3

Table 3 Calculation of average crystallite size of as fabricated CrO_3 thin films on FTO substrate using AACVD at 400°

Peak position 2θ (°)	**FWHM B_{size} (°)**	**Dp (nm)**	**Dp Average (nm)**
38.101	0.1574	55.79	53.04
54.582	0.2362	39.60	
61.629	0.3149	30.73	

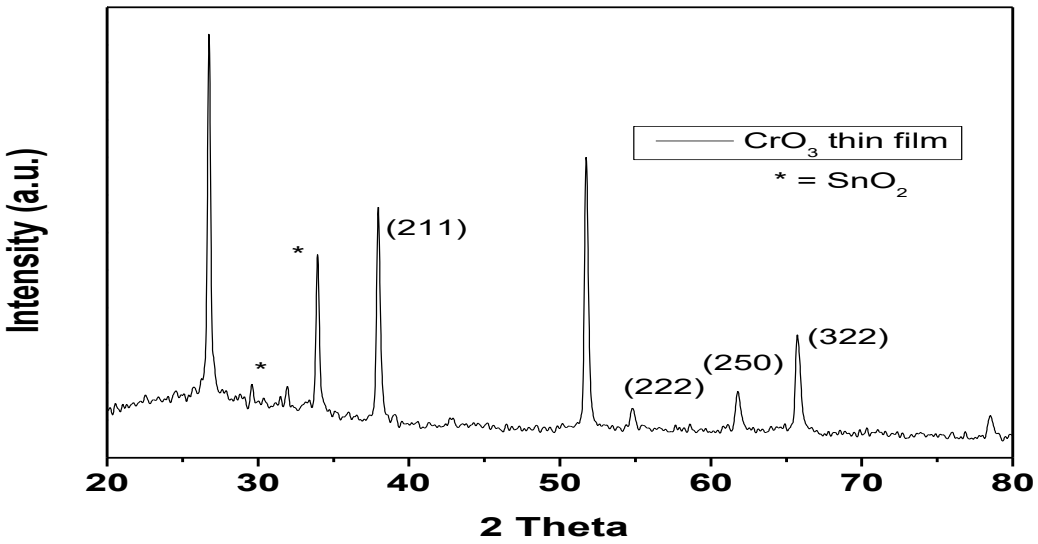

Figure 16 (a) XRD peaks pattern of as fabricate of CrO_3 film upon FTO substrate using AACVD at 400°

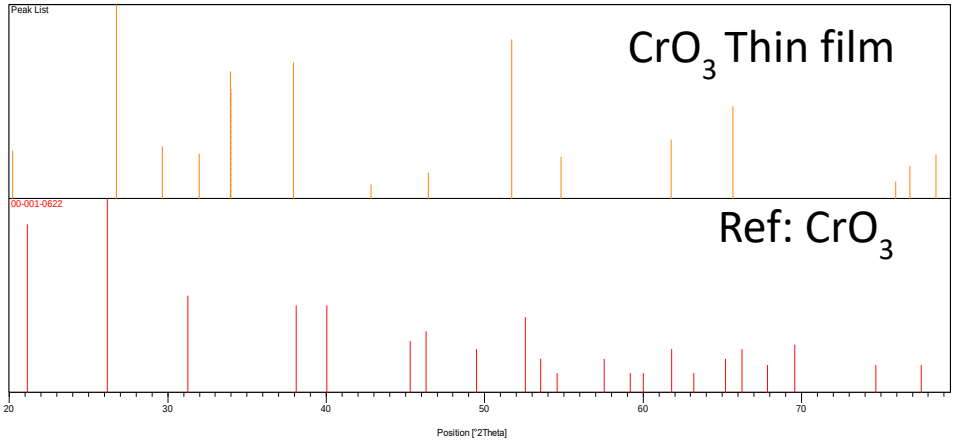

Figure16 (b) Matching of peaks with reference pattren for CrO_3

4.2 Functional Group Studies:

FTIR analysis was done to identify the presence of metal oxygen bond in the thin films of desired transition metal oxides.

4.2.1 Iron Oxide:

Observed values of FTIR bands are in the range of 520 and 692 cm^{-1} as shown in the Figure 17 and matched with the values cited in the literature for iron oxide.[87] These are associated with the Fe-O stretching vibrations present in the alpha phase hematite Fe_2O_3. No significant band present in the region from 1000 to 4000 cm^{-1} which indicates the absence of any impurity such as water or other organic impurities.

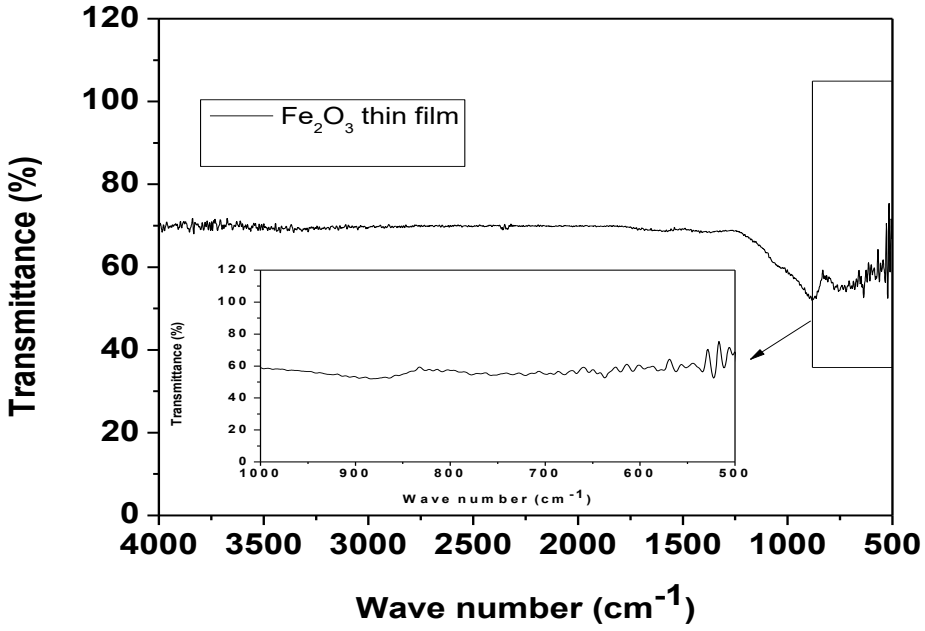

Figure 17 FTIR spectrum of as fabricated thin films of Fe_2O_3 upon FTO substrate using AACVD at 420°C

4.2.2 Yttrium Oxide:

Sharp band present around 530 cm^{-1} in FTIR spectrum is associated with the yttrium oxide; shows the Y-O vibrations and in accordance with the literature cited value[88]. Absence of any prominent band in the region onwards from 1000 to 4000 cm^{-1} indicated that the synthesized films are pure and free from impurities.

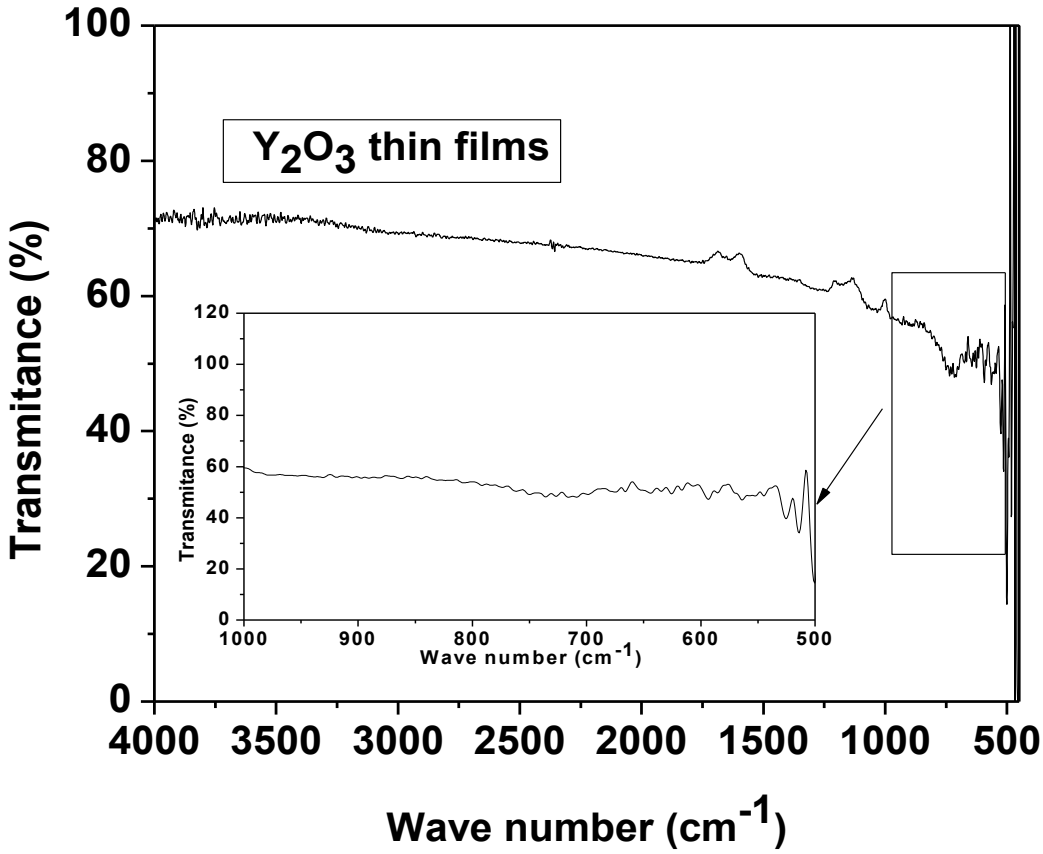

Figure 18 FTIR spectrum of as fabricated Y_2O_3 thin films upon FTO substrate using AACVD at 450°C

.

4.2.3 Chromium Oxide:

FTIR bands present in the range of 504 and 606 cm^{-1} perfectly matched with the data base values for Chromium oxide[89]. Again, no significance bands present apart from these, which is the indication of that the grown films are of pure metal oxide.

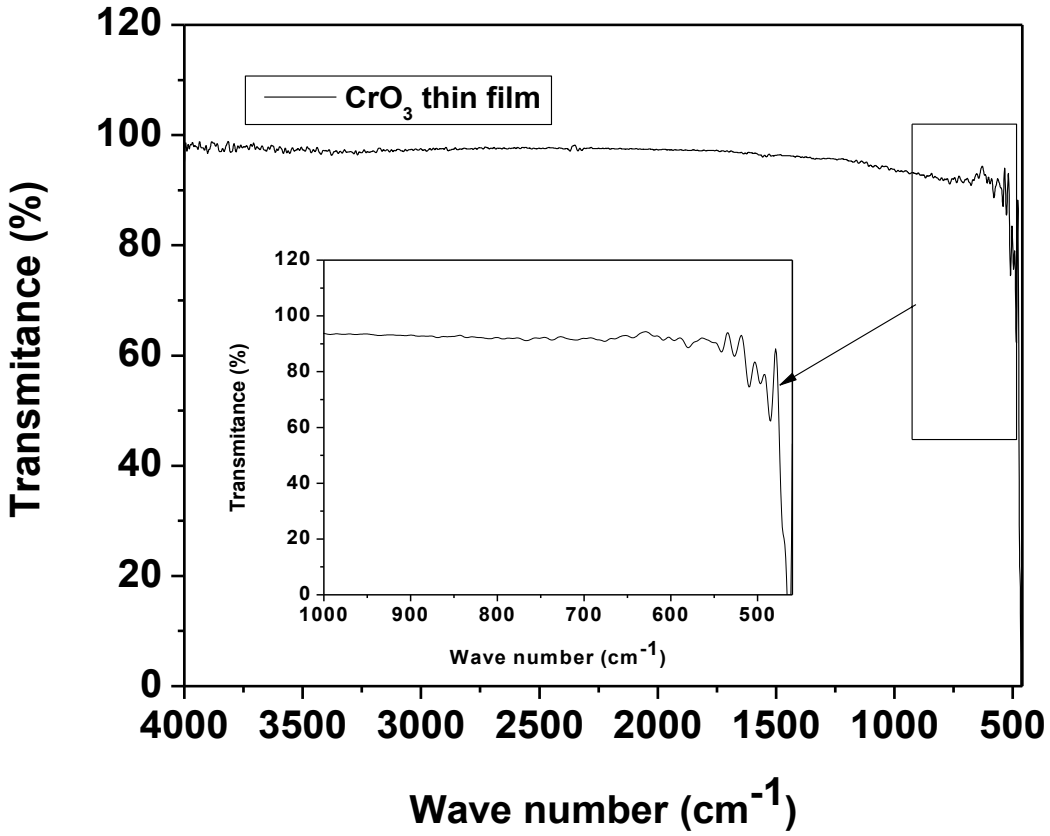

Figure 19 FTIR spectrum of as fabricated CrO_3 thin films upon FTO substrate using AACVD at 400°C

4.3 Morphological Analysis:

Field Emission Scanning electron microscopy i.e. (FESEM) images recorded at various scales were used to study the surface morphology and particle size of the deposited thin film.

4.3.1 Iron Oxide:

Figure 20 shows the FESEM images of as-fabricated Fe_2O_3 thin films on FTO substrate using single source precursor at 400 °C. It was observed that the surface of the thin films consists of small particle (i.e. ~ nanometer range) with random orientation and shape. The particle size of the grains is in the range of ~ 60−120 nm– having diameter of ~40−60 nm. The colonies of particles are expected to consist of small needle-like nanostructured and are formed due to agglomeration of these individual particles at the deposition temperature. Due to inter linking connection network of particles is formed which helps the fast transportation of charge carriers i.e. photoinduced charges. This is expected due to the generation of electronic connections among the inter-linked particles during the growth of Fe_2O_3 thin films. The particles at the surface of thin films are uniformly distributed to form a compact surface. The interlinked particles have the porous structure which resulted in high internal surface area of the films. It is evident that the presence of such structure enabled the unique chemical and physical properties of the films and are potential features of the films showing higher photoelectrochemical water splitting efficiency.

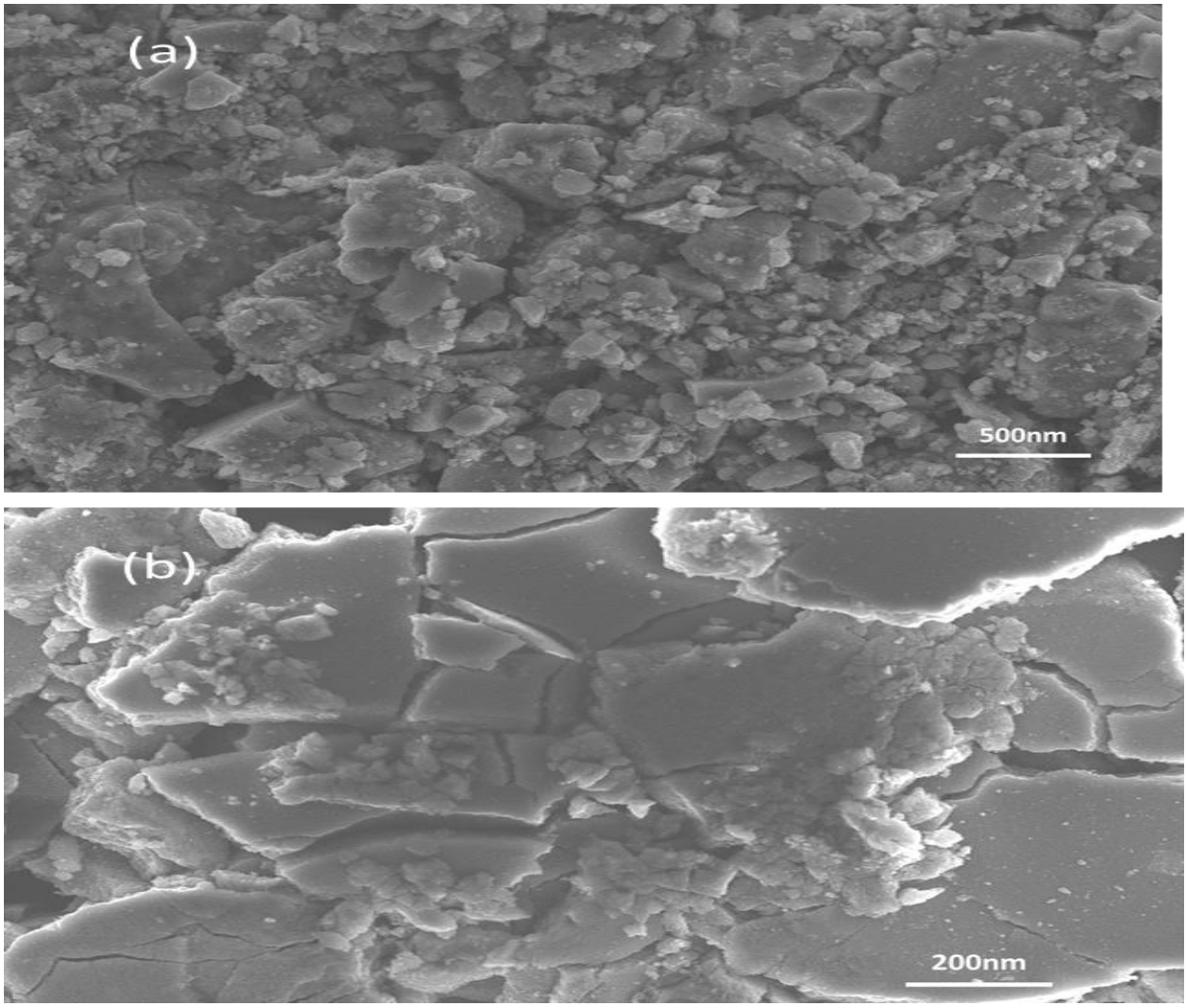

Figure 20 (a, b) Surface morphological study showing the FESEM images of Fe_2O_3 thin films at 420°C.

4.3.2 Yttrium Oxide:

Figure. 21 shows the FESEM images of the as-fabricated Y_2O_3 thin films deposited on the FTO substrate using AACVD. The surface of the films consisted of tiny particles with random orientation and are distributed throughout the surface of the films to form a compact and crack-free surface of the films. It is estimated that the particle sizes are in the range of ~ 80−150 nm–having diameter of ~60−100 nm. The surface roughness of the films is observed throughout the

surface due to grains inter-junctions with the substrate. The tightly packed thin films are free from cracks and pinhole due to random arrangement of particles and formed compact films.

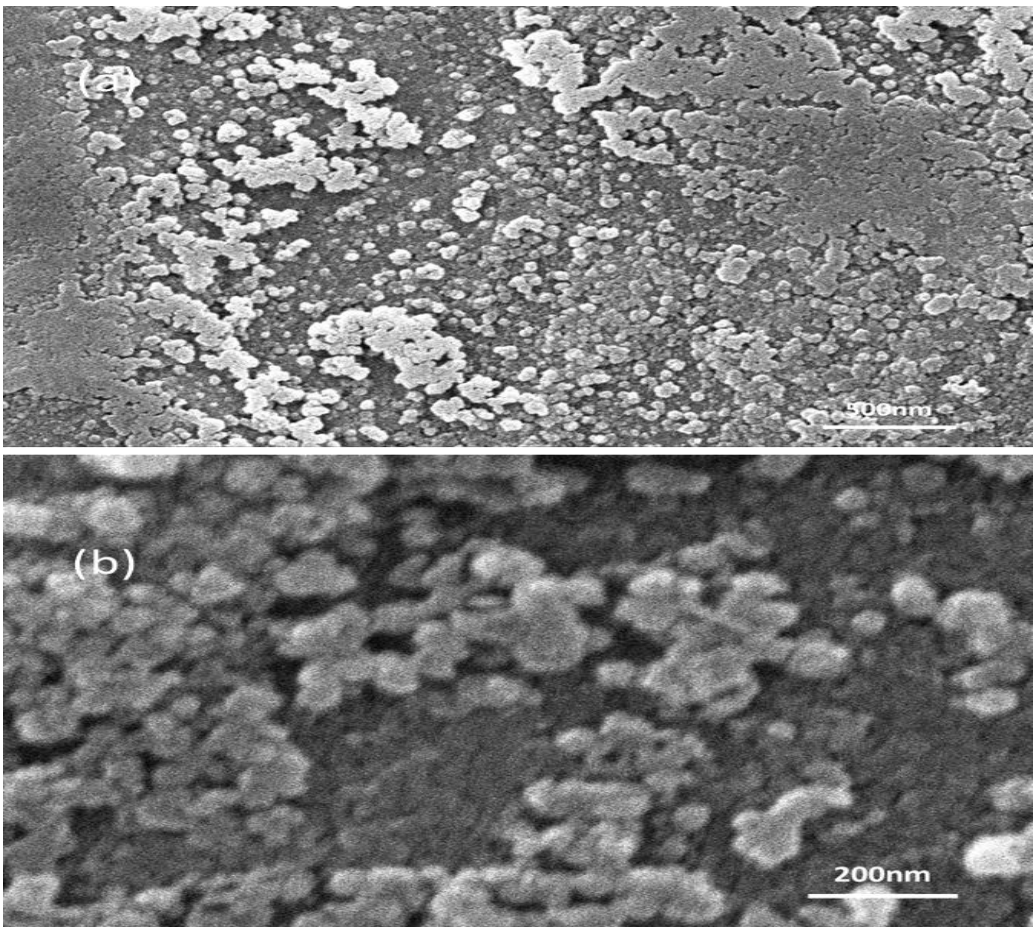

Figure 21 (a, b) Surface morphological studies showing the FESEM images of the Y_2O_3 thin films at 450°C.

4.3.3 Chromium Oxide:

Scanning electron microscope (FESEM) images of the CrO_3 thin films were examined to study the surface morphology and results are presented in Figure 22. The overview of the films surface morphology reveals the homogeneous and continuous distribution of the particles at the surface of the films. Deep analysis of the films confirmed the absence of any separate layer fabrication in films. The average crystallite size calculated using Scherer formula is different as compared to the grain size–which is expected because of the agglomeration of particles as can be seen from FESEM images.The single step growth of the thin films using AACVD made it more suitable technique for the fabrication of films for industrial applications. At the selected temperature, the grains agglomerated without fusion of the grains structure with marginal increase in the particle size.

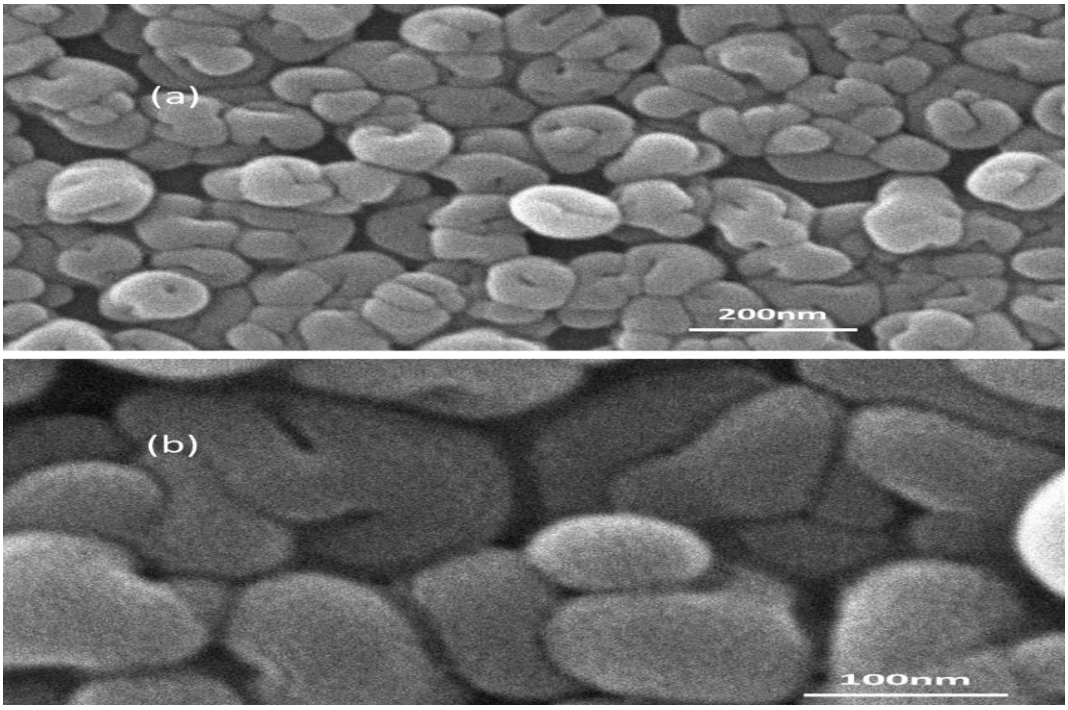

Figure 22 (a, b) Surface morphological studies showing the FESEM images of the CrO_3 thin films at 400°C.

4.4 Band Gap Studies:

Most interesting and critical issue for the practical application of the designed materials depends on the microstructure and chemical properties of the materials. Therefore, detailed study has been carried out to analyze the optical properties of the as-fabricated transition metal oxide thin films using defuse reflectance spectroscopy. UV–visible spectroscopy was run employing diffuse reflectance mode. For this, lymbda 950 UV–vis-NIR spectrophotometer was used, equipped with a Harrick Praying Mantis unit for calculating the diffuse reflectance spectra of prepared samples. Value of Band gap is influenced by various factors such as average crystal size, synthesis procedure of the metal semiconductor, roughness of surface, porosity of surface, grain size, and thickness. Furthermore, various methods for calculating the band gap from the UV–vis reflectance spectra are used. The optical band gap energy of the prepared thin films is calculated either by direct or indirect transition among the conduction and valence bands. The Kubelka–Munk function F(R); was used to estimate the transition between extended conduction and valence bands states. Relation between reflectance and Kubelka–Munk function is given in following equation.

$$F(R) = \frac{(1-R)^2}{2R}$$

Where, R and F(R) represents diffuse reflectance of the sample and Kubelka–Munk function, respectively. The band gap is calculated by the tauc-plot between square of modified Kubelka–Munk function F (R) against photon energy (hυ). Obtained values of band gap calculated by using above relation for the synthesized transition metal oxides thin films is discussed in following section.

4.4.1 Iron oxide:

Thin films of iron oxide (Fe_2O_3) prepared by using AACVD method of fabrication and deposited onto FTO substrate were red in color. Before performing the DRS of developed films bare FTO was run to remove background noise. The value was calculated by plotting a graph between square of F (R) and photon energy (Figure 23). The minimum value of band gap is calculated as 2.05 eV and is in accordance with the values cited in literature [90]. This confirms

the semiconductor behavior of the fabricated thin films. Furthermore, this values indicated that the prepared film can be employed for water splitting applications.

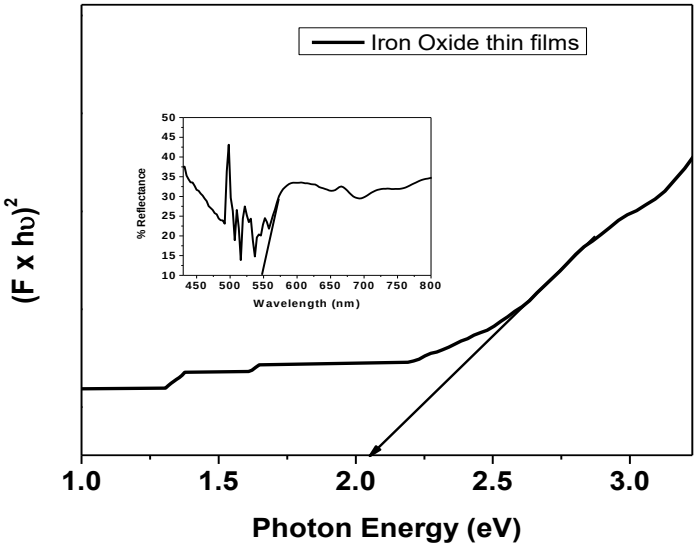

Figure 23 Band gap calculations of as fabricated Fe_2O_3 thin films upon FTO substrate using AACVD at 420°C inset shows the DRS spectra

4.4.2 Yttrium Oxide:

As discussed early, the yttrium oxide thin films have been fabricated on the FTO conducting glass substrate, the bare FTO was run to remove the background noise before performing the DRS spectra of the Y_2O_3 thin films. The as-fabricated Y_2O_3 thin films were transparent in appearance due to complete oxidation reaction of yttrium during the fabrication process using AACVD.

Figure 24 shows the plot of the F(R) against the band gap energy of the Y_2O_3 thin films. The bang gap energy of the Y_2O_3 thin films has been estimated from the extrapolation of the linear part to the energy axis to the zero, which is known as Kabulk functions. The estimated band gap energy of the Y_2O_3 thin films is ~ 3.3 eV which lower than the previously reported values. In literature different values of band gap of Y_2O_3 are cited which varies from 5.5 to 3.9 eV. It

is reported that in the case of polycrystalline thin films, the presence of higher concentration of the charge carrier and formation of potential barriers at the boundaries of the crystallite enhanced the band gap energy value. This means that the thin films have larger crystallite boundaries as compared to the crystallite size. Whereas, the presence of disorders and defects/vacancies in the thin films surface reduces the band gas energy value due to existence of the localized states. Thus, the lower band gap value of the as-fabricated Y_2O_3 thin films is expected due to the presence of disorder and defects in the thin films.

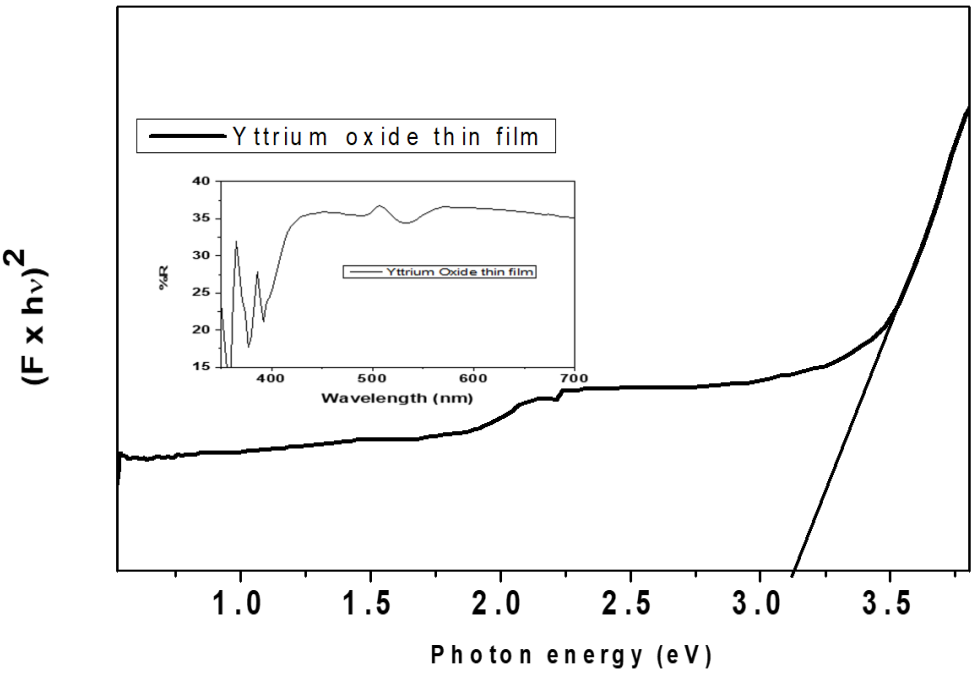

Figure 24 Band gap calculations of as fabricated Y_2O_3 thin film upon FTO substrate using AACVD at 450°C inset shows DRS spectra

4.4.3 Chromium Oxide

By following the same method as discussed in preceding; Calculated value of band gap chromium oxide (CrO_3) thin films is 2.75 eV. Band gap values of 4.32 eV, 3.14 and 2.25 eV is previously reported in literature [91] The reason in lowering of band gap is expected due to change in method of fabrication of films as well as change of substrate and deposition temperature. Furthermore, it is stated that with the increase in the grain size the band gap values of thin films lower down. As can be seen in the FESEM images (Figure. 22) the grain size of as-fabricated films of CrO_3 is relatively high. So, all these factors cause the reduction in band gap values. The lower band gap energy value of the thin films is expected to enhance its ability to absorb large portion of solar spectrum and can effectively use in water splitting application.

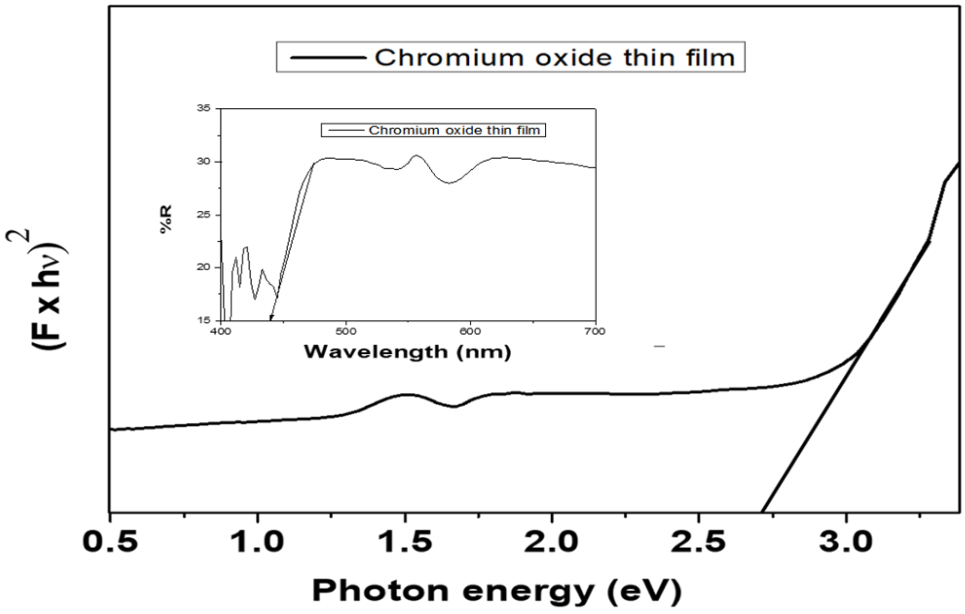

Figure 25 Band gap calculations of as fabricated CrO_3 thin film upon FTO substrate using AACVD at 400°C inset graph shows DRS spectra

4.5 Photoelectrochemical Studies:

PEC measurements were performed by means of a standard three-electrode arrangement of the transition metal oxide photoanode as working electrode, hydrogen as reference electrode, and with a Pt counter electrode in 1M solution of NaOH. Scan rate during the PEC measurements was 20 mV/s. The current response was calculated in the dark with the variation of applied potential. It was noted that no significant amount of current was produced at the applied potential of 1.4V. Then the PEC measurements were done under illumination of the coated side of the thin film through a Xe lamp (OPS-A500, Newport). A Xe lamp source having a power equals to 150 mW cm^{-2} was used. Area of electrode under light irradiation was almost 1 cm^2. The current–voltage measurement was recorded using potential difference Gammry 3000 potentiostate. The current voltage profile calculated in dark and under illumination of light is shown in the graphs. The axis bar represents the variation of applied voltage and current density along the X-axis and y-axis, respectively.

4.5.1 Iron Oxide:

Fe_2O_3 films showed negligible current in the dark. The illumination of the semiconducting electrode causes photogeneration of excess charge carriers and results in much increase in the amount of current produced a photocurrent density of 4 mA/cm^2 at 1.4V (Figure 26). The onset potential for these films is equal to 0.7 V. This current density response under simulated light well established that the prepared films photoanode had excellent light response and exceptional stability.

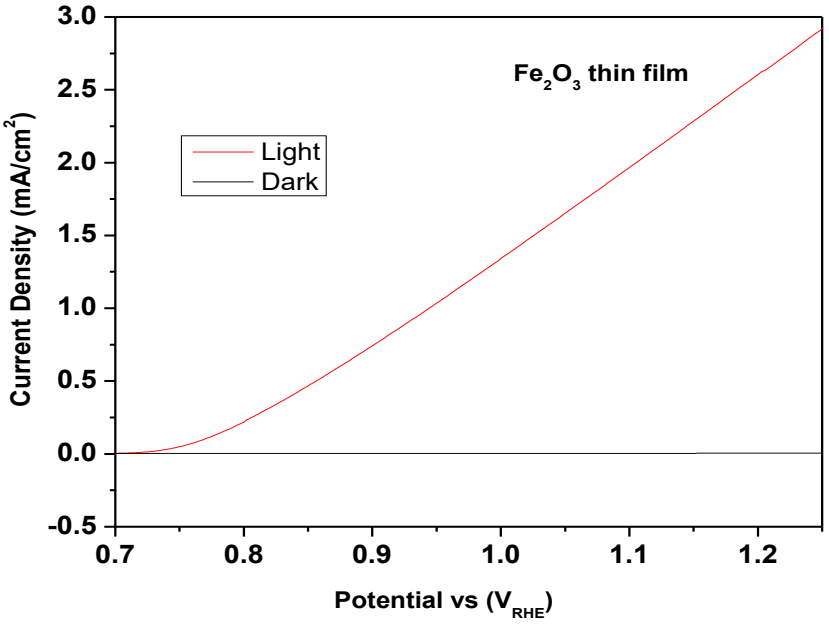

Figure 26 PEC current voltage curve of Fe_2O_3

4.5.3 Yttrium Oxide:

In case of yttrium oxide films, current response in dark and under light irradiation was calculated by the same procedure. The result obtained in this case is shown in Figure 27. Y_2O_3 thin films yielded amount of current which is equal to almost 0.6 mA/cm^2 under applied potential of 1.4 V while onset potential of the yttria films is 0.8 V.

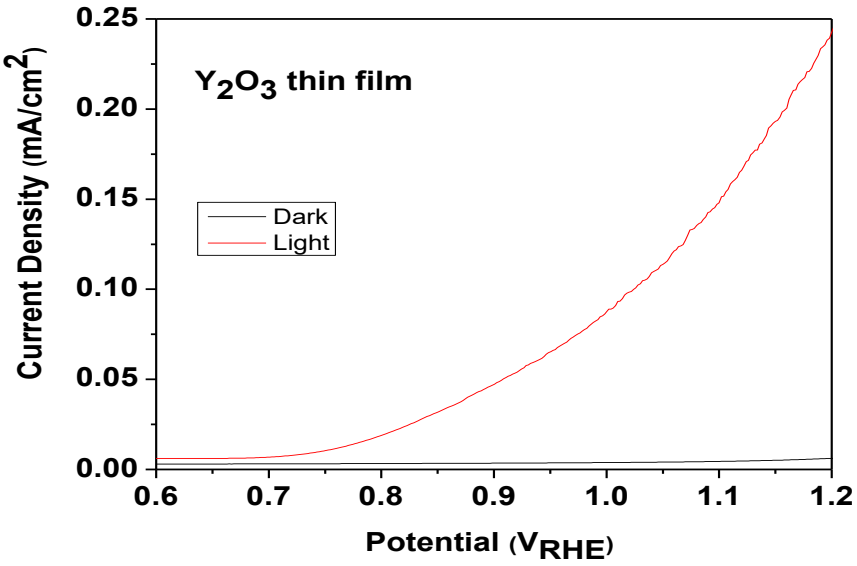

Figure 27 PEC current voltage curve of Y_2O_3

4.5.2 Chromium Oxide:

In Figure 28, J-V (current density vs applied potential) curves obtained for the CrO_3 thin films by following the aforementioned procedure is shown. It can be seen from the values obtained that the prepared films showed clear response towards the light. In the dark mode, no amount of current was produced. Whereas, under light irradiation, a current density equals to 1.75 mA/c cm^2 was observed at 1.4 V. The onset potential in this case is 0.8 V.

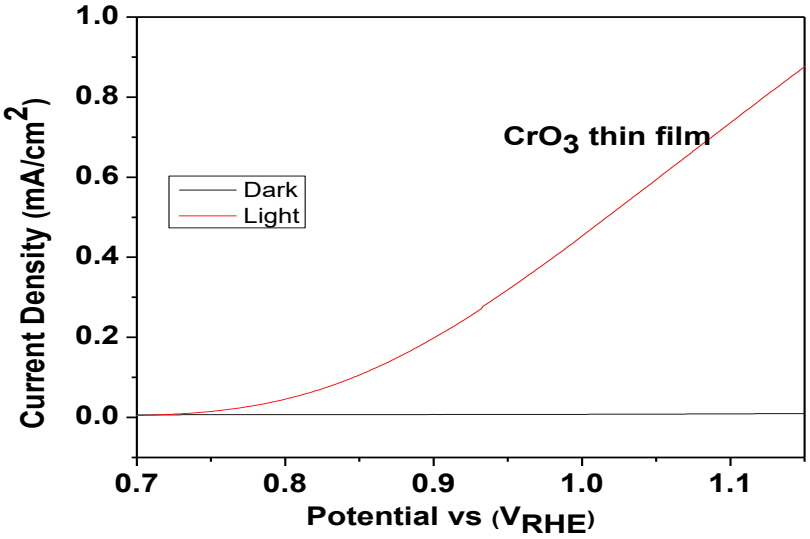

Figure 28 PEC current voltage curve f CrO_3

In the case of Fe_2O_3, the amount of current density produced is maximum while in case of yttrium it is minimum and of CrO_3 is in between these two. These results are in accordance to the band gap values calculated for the fabricated films using DRS as described above. Although the onset potential is almost similar for all 3 films difference in amount f produced current can be attributed to the factors such as the better rate charge generation in the case of Iron oxide thin films as compared to the other electrodes. The photoexcited charge carrier i.e. holes and electrons interact with the ions in the solution to start the redox reaction at their respective electrode with the liberation of gases. This proves that the presence of optimum band gap energy values played an important role in the PEC study of the fabricated thin films.

Conclusion

We have successfully synthesized the transition metal oxides thin films of iron, yttrium and chromium using AACVD from their respective single source precursors. These films were characterized for structural, optical and morphological study using different analytical techniques such as XRD, FTIR, FESEM and DRS. The XRD peak patterns of the respective thin films confirmed the successful formation of stable phase of the corresponding metal oxide. It was analyzed that the XRD peak pattern of the iron oxide thin film matched well with the reported pattern having alpha phase iron oxide Fe_2O_3 of rhombohedral structure. In the case of chromium oxide thin film, the XRD peak pattern matched with the CrO_3 phase with cubic structure having chromium in +6 oxidation. The Y_2O_3 thin films confirmed the presence of cubic structure. The estimated crystallite size confirmed the average size ranges for Fe_2O_3 and Y_2O_3. The FTIR spectra confirmed the absence of any organic impurity attached at the surface of the thin films and confirmed the presence of metal oxygen bond. The FESEM images of the thin films showed the presence of different grain boundary sizes. The particles are randomly distributed at the surface of the respective thin films except in the case of CrO_3, where particles showed unique type of distribution. The band gap energy values of as-fabricated thin films were estimated as. The calculated band gap energy values of the thin films fall in the range which is suitable for PEC water splitting. Finally, the prepared thin films were tested as working electrodes for their PEC water splitting potential through linear voltammeter. It was observed that the as-fabricated metal oxide thin films showed reasonable amount of current density generation under solar irradiation. In future, the prepared thin films will be studied for their electrochromic potential application.

References

[1] R. Baños, F. Manzano-Agugliaro, F.G. Montoya, C. Gil, A. Alcayde, J. Gómez, Optimization methods applied to renewable and sustainable energy: A review, Renew. Sustain. Energy Rev. 15 (2011) 1753–1766. https://doi.org/10.1016/j.rser.2010.12.008.

[2] B. Zohuri, P. McDaniel, Energy Resources and the Role of Nuclear Energy, in: Adv. Smaller Modul. React., Springer International Publishing, Cham, 2019: pp. 23–67. https://doi.org/10.1007/978-3-030-23682-3_2.

[3] M. Dehghani, Z. Montazeri, O.P. Malik, ENERGY COMMITMENT: A PLANNING OF ENERGY CARRIER BASED ON ENERGY CONSUMPTION, Electr. Eng. Electromechanics. (2019) 69–72. https://doi.org/10.20998/2074-272X.2019.4.10.

[4] S.E. Hosseini, M.A. Wahid, Hydrogen production from renewable and sustainable energy resources: Promising green energy carrier for clean development, Renew. Sustain. Energy Rev. 57 (2016) 850–866. https://doi.org/10.1016/j.rser.2015.12.112.

[5] S. Kouro, B. Wu, H. Abu-Rub, F. Blaabjerg, Photovoltaic Energy Conversion Systems, in: Power Electron. Renew. Energy Syst. Transp. Ind. Appl., John Wiley & Sons, Ltd, Chichester, UK, 2014: pp. 160–198. https://doi.org/10.1002/9781118755525.ch7.

[6] D.G. Nocera, On the future of global energy, Daedalus. 135 (2006) 112–115. https://doi.org/10.1162/daed.2006.135.4.112.

[7] M. Höök, X. Tang, Depletion of fossil fuels and anthropogenic climate change—A review, Energy Policy. 52 (2013) 797–809. https://doi.org/10.1016/j.enpol.2012.10.046.

[8] S. Becken, B. Mackey, What role for offsetting aviation greenhouse gas emissions in a deep-cut carbon world?, J. Air Transp. Manag. 63 (2017) 71–83. https://doi.org/10.1016/j.jairtraman.2017.05.009.

[9] T. Güney, Renewable energy, non-renewable energy and sustainable development, Int. J. Sustain. Dev. World Ecol. 26 (2019) 389–397. https://doi.org/10.1080/13504509.2019.1595214.

[10] Y. Zhao, T. Bostrom, Application of Ionic Liquids in Solar Cells and Batteries: A Review, Curr. Org. Chem. 19 (2015) 556–566. https://doi.org/10.2174/1385272819666150127002529.

[11] A. Kraft, Electrochromism: a fascinating branch of electrochemistry, ChemTexts. 5 (2019) 1. https://doi.org/10.1007/s40828-018-0076-x.

[12] B. Schwenzer, Chapter 3. Energy Conversion and Storage, in: 2019: pp. 125–166. https://doi.org/10.1039/9781788015806-00125.

[13] N.L. Panwar, S.C. Kaushik, S. Kothari, Role of renewable energy sources in environmental protection: A review, Renew. Sustain. Energy Rev. 15 (2011) 1513–1524. https://doi.org/10.1016/j.rser.2010.11.037.

[14] Y. Hames, K. Kaya, E. Baltacioglu, A. Turksoy, Analysis of the control strategies for fuel saving in the hydrogen fuel cell vehicles, Int. J. Hydrogen Energy. 43 (2018) 10810–10821. https://doi.org/10.1016/j.ijhydene.2017.12.150.

[15] J. Liao, H. Huang, Y. Chen, CO2 promotes the conjugative transfer of multiresistance genes by facilitating cellular contact and plasmid transfer, Environ. Int. 129 (2019) 333–342. https://doi.org/10.1016/j.envint.2019.05.060.

[16] N. Kannan, D. Vakeesan, Solar energy for future world: - A review, Renew. Sustain. Energy Rev. 62 (2016) 1092–1105. https://doi.org/10.1016/j.rser.2016.05.022.
[17] C. Tan, Q. Zhi, The Energy-water Nexus: A literature Review of the Dependence of Energy on Water, Energy Procedia. 88 (2016) 277–284. https://doi.org/10.1016/j.egypro.2016.06.154.
[18] A. FUJISHIMA, K. HONDA, Electrochemical Photolysis of Water at a Semiconductor Electrode, Nature. 238 (1972) 37–38. https://doi.org/10.1038/238037a0.
[19] Y. Qiu, Z. Pan, H. Chen, D. Ye, L. Guo, Z. Fan, S. Yang, Current progress in developing metal oxide nanoarrays-based photoanodes for photoelectrochemical water splitting, Sci. Bull. 64 (2019) 1348–1380. https://doi.org/10.1016/j.scib.2019.07.017.
[20] Y. Zhao, N. Hoivik, K. Wang, Recent advance on engineering titanium dioxide nanotubes for photochemical and photoelectrochemical water splitting, Nano Energy. 30 (2016) 728–744. https://doi.org/10.1016/j.nanoen.2016.09.027.
[21] P. Arunachalam, A.M. Al Mayouf, Photoelectrochemical Water Splitting, in: Noble Met. Oxide Hybrid Nanoparticles, Elsevier, 2019: pp. 585–606. https://doi.org/10.1016/B978-0-12-814134-2.00028-0.
[22] M. Zhou, X.W. (David) Lou, Y. Xie, Two-dimensional nanosheets for photoelectrochemical water splitting: Possibilities and opportunities, Nano Today. 8 (2013) 598–618. https://doi.org/10.1016/j.nantod.2013.12.002.
[23] R. Zan, A. Altuntepe, Nitrogen doping of graphene by CVD, J. Mol. Struct. 1199 (2020) 127026. https://doi.org/10.1016/j.molstruc.2019.127026.
[24] R. Haubner, The history of hard CVD coatings for tool applications at the University of Technology Vienna, Int. J. Refract. Met. Hard Mater. 41 (2013) 22–34. https://doi.org/10.1016/j.ijrmhm.2013.01.012.
[25] L. Meng, J. Feng, Y. Yu, W. Yan, H. Li, X. Wang, X. Yan, Formation mechanism of 2D WS2 with different morphology by chemical vapor deposition, Phys. E Low-Dimensional Syst. Nanostructures. 114 (2019) 113641. https://doi.org/10.1016/j.physe.2019.113641.
[26] H.M. Chen, C.K. Chen, R.-S. Liu, L. Zhang, J. Zhang, D.P. Wilkinson, Nano-architecture and material designs for water splitting photoelectrodes, Chem. Soc. Rev. 41 (2012) 5654. https://doi.org/10.1039/c2cs35019j.
[27] S.N. Ariffin, H.N. Lim, Z.A. Talib, A. Pandikumar, N.M. Huang, Aerosol-assisted chemical vapor deposition of metal oxide thin films for photoelectrochemical water splitting, Int. J. Hydrogen Energy. 40 (2015) 2115–2131. https://doi.org/10.1016/j.ijhydene.2014.11.131.
[28] A.A. Tahir, K.G.U. Wijayantha, M. Mazhar, V. McKee, ZnFe2O4 thin films from a single source precursor by aerosol assisted chemical vapour deposition, Thin Solid Films. 518 (2010) 3664–3668. https://doi.org/10.1016/j.tsf.2009.09.104.
[29] T. Stoycheva, F.E. Annanouch, I. Gràcia, E. Llobet, C. Blackman, X. Correig, S. Vallejos, Micromachined gas sensors based on tungsten oxide nanoneedles directly integrated via aerosol assisted CVD, Sensors Actuators B Chem. 198 (2014) 210–218. https://doi.org/10.1016/j.snb.2014.03.040.
[30] E. Callard preedy, P. Prokopovich, History of inhaler devices, in: Inhaler Devices, Elsevier, 2013: pp. 13–28. https://doi.org/10.1533/9780857098696.1.13.

[31] D. Zang, S. Tarafdar, Y.Y. Tarasevich, M. Dutta Choudhury, T. Dutta, Evaporation of a Droplet: From physics to applications, Phys. Rep. 804 (2019) 1–56. https://doi.org/10.1016/j.physrep.2019.01.008.
[32] P. Marchand, C.J. Carmalt, Molecular precursor approach to metal oxide and pnictide thin films, Coord. Chem. Rev. 257 (2013) 3202–3221. https://doi.org/10.1016/j.ccr.2013.01.030.
[33] A.A. Tahir, M.A. Ehsan, M. Mazhar, K.G.U. Wijayantha, M. Zeller, A.D. Hunter, Photoelectrochemical and Photoresponsive Properties of Bi 2 S 3 Nanotube and Nanoparticle Thin Films, Chem. Mater. 22 (2010) 5084–5092. https://doi.org/10.1021/cm101642b.
[34] G. Baldacchino, Water radiolysis with heavy-ion beams at GANIL. Back to 20 years of investigations, J. Phys. Conf. Ser. 629 (2015) 012009. https://doi.org/10.1088/1742-6596/629/1/012009.
[35] S. Le Caër, L. Dezerald, K. Boukari, M. Lainé, S. Taupin, R.M. Kavanagh, C.S.N. Johnston, E. Foy, T. Charpentier, K.J. Krakowiak, R.J.-M. Pellenq, F.J. Ulm, G.A. Tribello, J. Kohanoff, A. Saúl, Production of H 2 by water radiolysis in cement paste under electron irradiation: A joint experimental and theoretical study, Cem. Concr. Res. 100 (2017) 110–118. https://doi.org/10.1016/j.cemconres.2017.05.022.
[36] L. Frances, M. Grivet, J.-P. Renault, J.-E. Groetz, D. Ducret, Hydrogen radiolytic release from zeolite 4A/water systems under γ irradiations, Radiat. Phys. Chem. 110 (2015) 6–11. https://doi.org/10.1016/j.radphyschem.2015.01.008.
[37] A.M. Abdalla, S. Hossain, O.B. Nisfindy, A.T. Azad, M. Dawood, A.K. Azad, Hydrogen production, storage, transportation and key challenges with applications: A review, Energy Convers. Manag. 165 (2018) 602–627. https://doi.org/10.1016/j.enconman.2018.03.088.
[38] Z. Wang, R.R. Roberts, G.F. Naterer, K.S. Gabriel, Comparison of thermochemical, electrolytic, photoelectrolytic and photochemical solar-to-hydrogen production technologies, Int. J. Hydrogen Energy. 37 (2012) 16287–16301. https://doi.org/10.1016/j.ijhydene.2012.03.057.
[39] A. KOGAN, Direct solar thermal splitting of water and on-site separation of the products?II. Experimental feasibility study, Int. J. Hydrogen Energy. 23 (1998) 89–98. https://doi.org/10.1016/S0360-3199(97)00038-4.
[40] E. Tezel, H.E. Figen, S.Z. Baykara, Hydrogen production by methane decomposition using bimetallic Ni–Fe catalysts, Int. J. Hydrogen Energy. 44 (2019) 9930–9940. https://doi.org/10.1016/j.ijhydene.2018.12.151.
[41] K. Paramesh, T. Chandrasekhar, Improvement of photobiological hydrogen production in Chlorococcum minutum using various oxygen scavengers, Int. J. Hydrogen Energy. (2019). https://doi.org/10.1016/j.ijhydene.2019.05.216.
[42] S. Shiva Kumar, V. Himabindu, Hydrogen production by PEM water electrolysis – A review, Mater. Sci. Energy Technol. 2 (2019) 442–454. https://doi.org/10.1016/j.mset.2019.03.002.
[43] J. Hnát, M. Plevova, R.A. Tufa, J. Zitka, M. Paidar, K. Bouzek, Development and testing of a novel catalyst-coated membrane with platinum-free catalysts for alkaline water electrolysis, Int. J. Hydrogen Energy. 44 (2019) 17493–17504.

https://doi.org/10.1016/j.ijhydene.2019.05.054.
[44] K. Zhang, M. Ma, P. Li, D.H. Wang, J.H. Park, Water Splitting Progress in Tandem Devices: Moving Photolysis beyond Electrolysis, Adv. Energy Mater. 6 (2016) 1600602. https://doi.org/10.1002/aenm.201600602.
[45] J. Joy, J. Mathew, S.C. George, Nanomaterials for photoelectrochemical water splitting – review, Int. J. Hydrogen Energy. 43 (2018) 4804–4817. https://doi.org/10.1016/j.ijhydene.2018.01.099.
[46] C. Gadiyar, A. Loiudice, R. Buonsanti, Colloidal nanocrystals for photoelectrochemical and photocatalytic water splitting, J. Phys. D. Appl. Phys. 50 (2017) 074006. https://doi.org/10.1088/1361-6463/aa50cd.
[47] S.K. Saraswat, D.D. Rodene, R.B. Gupta, Recent advancements in semiconductor materials for photoelectrochemical water splitting for hydrogen production using visible light, Renew. Sustain. Energy Rev. 89 (2018) 228–248. https://doi.org/10.1016/j.rser.2018.03.063.
[48] T. Hayashi, R. Niishiro, H. Ishihara, M. Yamaguchi, Q. Jia, Y. Kuang, T. Higashi, A. Iwase, T. Minegishi, T. Yamada, K. Domen, A. Kudo, Powder-based (CuGa 1−y In y) 1−x Zn 2x S 2 solid solution photocathodes with a largely positive onset potential for solar water splitting, Sustain. Energy Fuels. 2 (2018) 2016–2024. https://doi.org/10.1039/C8SE00079D.
[49] T.D. Lee, A.U. Ebong, A review of thin film solar cell technologies and challenges, Renew. Sustain. Energy Rev. 70 (2017) 1286–1297. https://doi.org/10.1016/j.rser.2016.12.028.
[50] F. Meillaud, M. Boccard, G. Bugnon, M. Despeisse, S. Hänni, F.-J. Haug, J. Persoz, J.-W. Schüttauf, M. Stuckelberger, C. Ballif, Recent advances and remaining challenges in thin-film silicon photovoltaic technology, Mater. Today. 18 (2015) 378–384. https://doi.org/10.1016/j.mattod.2015.03.002.
[51] L. Petti, N. Münzenrieder, C. Vogt, H. Faber, L. Büthe, G. Cantarella, F. Bottacchi, T.D. Anthopoulos, G. Tröster, Metal oxide semiconductor thin-film transistors for flexible electronics, Appl. Phys. Rev. 3 (2016) 021303. https://doi.org/10.1063/1.4953034.
[52] N. Setter, D. Damjanovic, L. Eng, G. Fox, S. Gevorgian, S. Hong, A. Kingon, H. Kohlstedt, N.Y. Park, G.B. Stephenson, I. Stolitchnov, A.K. Taganstev, D. V. Taylor, T. Yamada, S. Streiffer, Ferroelectric thin films: Review of materials, properties, and applications, J. Appl. Phys. 100 (2006) 051606. https://doi.org/10.1063/1.2336999.
[53] M.R. Kasaai, Zein and zein -based nano-materials for food and nutrition applications: A review, Trends Food Sci. Technol. 79 (2018) 184–197. https://doi.org/10.1016/j.tifs.2018.07.015.
[54] R. Li, F. Xiao, S. Amirkhanian, Z. You, J. Huang, Developments of nano materials and technologies on asphalt materials – A review, Constr. Build. Mater. 143 (2017) 633–648. https://doi.org/10.1016/j.conbuildmat.2017.03.158.
[55] W. Li, P. Liu, P.K. Liaw, Microstructures and properties of high-entropy alloy films and coatings: a review, Mater. Res. Lett. 6 (2018) 199–229. https://doi.org/10.1080/21663831.2018.1434248.
[56] P. Brack, J.S. Sagu, T.A.N. Peiris, A. McInnes, M. Senili, K.G.U. Wijayantha, F. Marken, E. Selli, Aerosol-Assisted CVD of Bismuth Vanadate Thin Films and Their

Photoelectrochemical Properties, Chem. Vap. Depos. 21 (2015) 41–45. https://doi.org/10.1002/cvde.201407142.
[57] Y. Yang, S. Niu, D. Han, T. Liu, G. Wang, Y. Li, Progress in Developing Metal Oxide Nanomaterials for Photoelectrochemical Water Splitting, Adv. Energy Mater. 7 (2017) 1700555. https://doi.org/10.1002/aenm.201700555.
[58] Z. Wang, L. Wang, Progress in designing effective photoelectrodes for solar water splitting, Chinese J. Catal. 39 (2018) 369–378. https://doi.org/10.1016/S1872-2067(17)62998-X.
[59] W. Septina, S.D. Tilley, Emerging Earth-abundant materials for scalable solar water splitting, Curr. Opin. Electrochem. 2 (2017) 120–127. https://doi.org/10.1016/j.coelec.2017.03.010.
[60] J. Jian, G. Jiang, R. van de Krol, B. Wei, H. Wang, Recent advances in rational engineering of multinary semiconductors for photoelectrochemical hydrogen generation, Nano Energy. 51 (2018) 457–480. https://doi.org/10.1016/j.nanoen.2018.06.074.
[61] S.N.H. Jaafar, L.J. Minggu, K. Arifin, M.B. Kassim, W.R.D. Wan, Natural dyes as TIO2 sensitizers with membranes for photoelectrochemical water splitting: An overview, Renew. Sustain. Energy Rev. 78 (2017) 698–709. https://doi.org/10.1016/j.rser.2017.04.118.
[62] S. JIULONG, DEVELOPMENT OF INORGANIC-ORGANIC HYBRID MATERIALS FOR WASTE WATER TREATMENT, 2014.
[63] Q. Ding, B. Song, P. Xu, S. Jin, Efficient Electrocatalytic and Photoelectrochemical Hydrogen Generation Using MoS 2 and Related Compounds, Chem. 1 (2016) 699–726. https://doi.org/10.1016/j.chempr.2016.10.007.
[64] Z. Chen, X. Duan, W. Wei, S. Wang, B.-J. Ni, Recent advances in transition metal-based electrocatalysts for alkaline hydrogen evolution, J. Mater. Chem. A. 7 (2019) 14971–15005. https://doi.org/10.1039/C9TA03220G.
[65] F. Yu, H. Zhou, Z. Zhu, J. Sun, R. He, J. Bao, S. Chen, Z. Ren, Three-Dimensional Nanoporous Iron Nitride Film as an Efficient Electrocatalyst for Water Oxidation, ACS Catal. 7 (2017) 2052–2057. https://doi.org/10.1021/acscatal.6b03132.
[66] J. Xie, S. Li, X. Zhang, J. Zhang, R. Wang, H. Zhang, B. Pan, Y. Xie, Atomically-thin molybdenum nitride nanosheets with exposed active surface sites for efficient hydrogen evolution, Chem. Sci. 5 (2014) 4615–4620. https://doi.org/10.1039/C4SC02019G.
[67] N. Han, P. Liu, J. Jiang, L. Ai, Z. Shao, S. Liu, Recent advances in nanostructured metal nitrides for water splitting, J. Mater. Chem. A. 6 (2018) 19912–19933. https://doi.org/10.1039/C8TA06529B.
[68] S. Rai, A. Ikram, S. Sahai, S. Dass, R. Shrivastav, V.R. Satsangi, CNT based photoelectrodes for PEC generation of hydrogen: A review, Int. J. Hydrogen Energy. 42 (2017) 3994–4006. https://doi.org/10.1016/j.ijhydene.2016.10.024.
[69] M.M. Momeni, Y. Ghayeb, Fabrication, characterization and photoelectrochemical performance of chromium-sensitized titania nanotubes as efficient photoanodes for solar water splitting, J. Solid State Electrochem. 20 (2016) 683–689. https://doi.org/10.1007/s10008-015-3093-3.
[70] S. Ismail, F.I.A. Bakar, N.N. Ahmad, Synthesis of Fe2O3/MWCNTs composite by oxidation and spin coating, in: 2019: p. 020092. https://doi.org/10.1063/1.5089391.

[71] A. Kusior, A. Wnuk, A. Trenczek-Zajac, K. Zakrzewska, M. Radecka, TiO2 nanostructures for photoelectrochemical cells (PECs), Int. J. Hydrogen Energy. 40 (2015) 4936–4944. https://doi.org/10.1016/j.ijhydene.2015.01.103.
[72] Z. Dong, D. Ding, T. Li, C. Ning, Facile preparation of Ti3+/Ni co-doped TiO2 nanotubes photoanode for efficient photoelectrochemical water splitting, Appl. Surf. Sci. 480 (2019) 219–228. https://doi.org/10.1016/j.apsusc.2019.02.237.
[73] M. Sluban, P. Umek, Role of Water in the Transformation of Protonated Titanate Nanoribbons to Anatase Nanoribbons, J. Phys. Chem. C. (2019) acs.jpcc.9b08225. https://doi.org/10.1021/acs.jpcc.9b08225.
[74] W. Wang, J. Dong, X. Ye, Y. Li, Y. Ma, L. Qi, Heterostructured TiO 2 Nanorod@Nanobowl Arrays for Efficient Photoelectrochemical Water Splitting, Small. 12 (2016) 1469–1478. https://doi.org/10.1002/smll.201503553.
[75] H.R. Khan, B. Akram, M. Aamir, M.A. Malik, A.A. Tahir, M.A. Choudhary, J. Akhtar, Fabrication of Ni2+ incorporated ZnO photoanode for efficient overall water splitting, Appl. Surf. Sci. 490 (2019) 302–308. https://doi.org/10.1016/j.apsusc.2019.06.078.
[76] R. Kant, C. Dwivedi, S. Pathak, V. Dutta, Fabrication of ZnO nanostructures using Al doped ZnO (AZO) templates for application in photoelectrochemical water splitting, Appl. Surf. Sci. 447 (2018) 200–212. https://doi.org/10.1016/j.apsusc.2018.03.208.
[77] P. Dias, L. Andrade, A. Mendes, Hematite-based photoelectrode for solar water splitting with very high photovoltage, Nano Energy. 38 (2017) 218–231. https://doi.org/10.1016/j.nanoen.2017.05.051.
[78] J.S. Kang, Y. Noh, J. Kim, H. Choi, T.H. Jeon, D. Ahn, J.-Y. Kim, S.-H. Yu, H. Park, J.-H. Yum, W. Choi, D.C. Dunand, H. Choe, Y.-E. Sung, Iron Oxide Photoelectrode with Multidimensional Architecture for Highly Efficient Photoelectrochemical Water Splitting, Angew. Chemie Int. Ed. 56 (2017) 6583–6588. https://doi.org/10.1002/anie.201703326.
[79] N. Kodan, K. Agarwal, B.R. Mehta, All-Oxide α-Fe 2 O 3 /H:TiO 2 Heterojunction Photoanode: A Platform for Stable and Enhanced Photoelectrochemical Performance through Favorable Band Edge Alignment, J. Phys. Chem. C. 123 (2019) 3326–3335. https://doi.org/10.1021/acs.jpcc.8b10794.
[80] L. Yang, H. Zhou, T. Fan, D. Zhang, Semiconductor photocatalysts for water oxidation: current status and challenges, Phys. Chem. Chem. Phys. 16 (2014) 6810. https://doi.org/10.1039/c4cp00246f.
[81] C. Fàbrega, S. Murcia-López, D. Monllor-Satoca, J.D. Prades, M.D. Hernández-Alonso, G. Penelas, J.R. Morante, T. Andreu, Efficient WO3 photoanodes fabricated by pulsed laser deposition for photoelectrochemical water splitting with high faradaic efficiency, Appl. Catal. B Environ. 189 (2016) 133–140. https://doi.org/10.1016/j.apcatb.2016.02.047.
[82] W. Shi, H. Li, J. Chen, X. Lv, Y. Shen, Hierarchical WO 3 nanoflakes architecture with enhanced photoelectrochemical activity, Electrochim. Acta. 225 (2017) 473–481. https://doi.org/10.1016/j.electacta.2016.12.166.
[83] X. Liu, Y. Liu, J. Su, M. Li, L. Guo, Facile preparation of BiVO4 nanoparticle film by electrostatic spray pyrolysis for photoelectrochemical water splitting, Int. J. Hydrogen Energy. 40 (2015) 12964–12972. https://doi.org/10.1016/j.ijhydene.2015.08.015.

[84] I. Khan, S. Ali, M. Mansha, A. Qurashi, Sonochemical assisted hydrothermal synthesis of pseudo-flower shaped Bismuth vanadate (BiVO 4) and their solar-driven water splitting application, Ultrason. Sonochem. 36 (2017) 386–392. https://doi.org/10.1016/j.ultsonch.2016.12.014.
[85] A. Angeloski, A.R. Gentle, J.A. Scott, M.B. Cortie, J.M. Hook, M.T. Westerhausen, M. Bhadbhade, A.T. Baker, A.M. McDonagh, From Lead(II) Dithiocarbamate Precursors to a Fast Response PbS Positive Temperature Coefficient Thermistor, Inorg. Chem. 57 (2018) 2132–2140. https://doi.org/10.1021/acs.inorgchem.7b03009.
[86] M.D. Regulacio, N. Tomson, S.L. Stoll, Dithiocarbamate Precursors for Rare-Earth Sulfides, Chem. Mater. 17 (2005) 3114–3121. https://doi.org/10.1021/cm0478071.
[87] ATR-FT-IR spectra of Iron(III) oxide (Fe2O3), (n.d.). http://lisa.chem.ut.ee/IR_spectra/paint/fillers/ironiii-oxide/.
[88] G. Alarcón-Flores, M. Aguilar-Frutis, M. García-Hipolito, J. Guzmán-Mendoza, M.A. Canseco, C. Falcony, Optical and structural characteristics of Y2O3 thin films synthesized from yttrium acetylacetonate, J. Mater. Sci. 43 (2008) 3582–3588. https://doi.org/10.1007/s10853-008-2566-5.
[89] ATR-FT-IR spectra of Chromium oxide (Cr2O3), (2015). http://lisa.chem.ut.ee/IR_spectra/paint/pigments/chromium-oxide/.
[90] A. Lassoued, B. Dkhil, A. Gadri, S. Ammar, Control of the shape and size of iron oxide (α-Fe2O3) nanoparticles synthesized through the chemical precipitation method, Results Phys. 7 (2017) 3007–3015. https://doi.org/10.1016/j.rinp.2017.07.066.
[91] H.-J. Zhai, S. Li, D.A. Dixon, L.-S. Wang, Probing the Electronic and Structural Properties of Chromium Oxide Clusters (CrO 3) n − and (CrO 3) n (n = 1–5): Photoelectron Spectroscopy and Density Functional Calculations, J. Am. Chem. Soc. 130 (2008) 5167–5177. https://doi.org/10.1021/ja077984d.